Global-scale Observations of the Limb and Disk (GOLD)

Release Notes

Revision 5.7 – September 13, 2024

Changes

Revision	Date	Changes
1.0	2/28/2019	Initial release
1.1	5/14/2019	Added "Incorrect Radiance values for the Night observations" to Known Issues
2.0	6/3/2019	Fixed issue with L1C NI1 data product and updated L1C NI1 and L1D NI1 to version 02.
		Initial limited release of Level 2 data products.
3.0	9/16/2019	New version of all L1C products with flatfield correction applied. Improved background subtraction algorithm for L1C OCC product.
		Release of additional L2 data products:
		TDISK, ON2, TLIMB and O2DEN through Aug 13, 2019 (with some exceptions, as noted below).
		QEUV through Jan 31, 2019.
3.1	12/6/2019	Added L1C and L1D Channel B NI1 data products to released products. See updated section 3.1.5 for more details.
		Added additional sections to Level 1 known issues:
		3.1.12 No High Particle Background Flag
		3.1.13 Incorrect Background Subtraction in Day and Night Scans
		3.1.14 Incorrect variable names and units in L1C occultation files
		3.1.15 Irradiance values in L1C occultation files are too large
3.2	4/8/2020	Added L2 NMAX data product to released products.
		Updated L2 TLIMB product to version 03.
		Added additional sections to Level 2 known issues:
		3.2.4.5 Look up table constraints (ON2)
		3.2.4.7 Flat Field correction artifacts (ON2)

		3.2.5.5 Flat Field correction artifacts (QEUV)
		3.2.6 Issues with NMAX data
3.3	4/16/2020	Updated section 3.2.6 Issues with NMAX data
3.4	8/28/2020	Added additional sections to Level 1 known issues:
		3.1.16 Field emission type events
		3.1.17 Effect of stars on the brightness
		Added additional section to Level 2 known issues:
		3.2.6.1 Model uncertainty (NMAX)
3.5	9/22/2020	Added additional image to Figure 3-10
		Added additional gaps in data for TDISK (3.2.3.7), ON2 (3.2.4.6), and NMAX (3.2.6.1).
3.6	10/22/2020	Added additional gaps in data for TDISK (3.2.3.7), ON2 (3.2.4.6), and NMAX (3.2.6.1).
3.7	11/19/2020	Added additional gaps in data for ON2 (3.2.4.6) and NMAX (3.2.6.1)
		Added additional sections to known issues:
		3.1.18 Horizontal artifacts in CHB NI1 scans
		3.2.6.3 Flat Field correction artifacts (NMAX)
3.8	11/24/2020	Updated known issues:
		3.1.4 Flatfield correction
		3.2.4.7 Flat Field correction artifacts (ON2)
4.0	4/2/2021	New versions of all L1C and L2 data products
		Updated "Known Issues" based on latest data
4.1	6/24/2021	Added additional GYM actuation dates to Table 3-1
		Updated section 3.1.17
		Added additional section to Level 1 known issues:
		3.1.22 Vertical depletion artifacts in NI1 data
4.2	9/14/2021	Added additional GYM actuation date to Table 3-1
		Updated figures 3-21, 3-22, and 3-24
		Added additional section to L2 known issues:
		3.2.6.3 Vertical Depletion Artifacts (NMAX)

4.3	9/27/2021	Updated sections 2 and 3.1.1 with information regarding changes to the Channel A observation cadence.
		Updated figures 3-21, 3-22, and 3-24
4.4	11/17/2021	Added additional GYM actuation date to Table 3-1
		Updated Level 2 O2DEN product to version 04 (see section 2.2.6)
4.5	8/5/2022	Added additional GYM actuation date to Table 3-1
		Updated Level 2 TDISK product to version 04 (see sections 2.2.3, 2.2.7, and 3.2.3)
4.6	9/6/2022	Added additional GYM actuation date to Table 3-1
		Updated figures 3-21, 3-22, and 3-24
5.0	5/26/2023	New versions of all L1C and L2 data products
		Updated "Known Issues" based on latest data
5.1	6/16/2023	Added additional GYM actuation date to Table 3-1
		Added additional section to Level 2 known issues:
		3.2.4.6 ON2 Artifacts during May 20-25, 2023
		3.2.5.6 Downward trend in QEUV beginning May 1, 2023
5.2	6/21/2023	Updated Level 2 GYM shift plots (figures 3-19, 3-20, and 3-22)
5.3	1/3/2024	Added additional GYM actuation dates to Table 3-1
		Updated Level 2 GYM shift plots (figures 3-19, 3-20, and 3-22)
		Removed Level 2 known issue: 3.2.5.6 Downward trend in QEUV beginning May 1, 2023
5.4	1/22/2024	Updated Level 2 GYM shift plots (figures 3-19, 3-20, and 3-22)
5.5	4/10/2024	Updated Level 2 ON2 version 04 data product to revision 02 (see section 2.2.4)
		Updated Level 2 TDISK version 05 data product to revision 02 (see sections 2.2.4 and 2.2.5)
5.6	5/20/2024	Added additional GYM actuation date to Table 3-1
		Updated Level 2 GYM shift plots (figures 3-19, 3-20, and 3-22)

| 5.7 | 9/13/2024 | Updated Level 2 NMAX data product to version 04 (see section 2.2.6) |

Table of Contents

1 Data Products:

This release includes new versions of all Level 1C (L1C) and Level 2 (L2) data products. Table 1-1 below provides the list of Version and Revision numbers associated with each data product for this release. The released dates of current GOLD data products can be found at https://gold.cs.ucf.edu/data/current-data-product-versions/

We refer users of these data products to the "**GOLD Science Data Product Guide**", available at https://gold.cs.ucf.edu/documentation/ for details about how these were obtained, and about their file format and content.

Data Product	Version Number	Revision Number
L1C: DAY	04	01
L1C: LIM	04	01
L1C: OCC	04	01
L1C: NI1	05	01
L1D: DAY	04	01
L1D: LIM	04	01
L1D: OCC	04	01
L1D: NI1	05	01
L2: NMAX	04	01
L2: O2DEN	05	01
L2: ON2	04	02
L2: QEUV	03	01
L2: TDISK	05	02
L2: TLIMB	05	01

Table 1-1 Version/Revision Numbers by Data Product for this Release

Update 4/10/2024: L2 TDISK version 05 and L2 ON2 version 04 have both been updated to revision 02. See sections 2, 2.2.4, and 2.2.5 for details.

Update 9/13/2024: L2 NMAX has been updated to version 04. See sections 2 and 2.2.6 for details.

2 Updates with This Release:

This release combines a full reprocess of all Level 1 and Level 2 data products. The major Level 1 changes that users should be aware of include improved temporal and geolocation accuracy, an improved flatfield correction algorithm, improved airglow subtraction for night-side occultations, and the addition of a new dark limb (DLM) observation type. All Level 1 changes are described in detail in section 2.1. All Level 2 data products were reprocessed using this new version of L1C data. This version also updates the scale height constant used in the algorithm for

the NMAX data product, as described in section 2.2. No other Level 2 algorithms were changed in this release.

Update 4/10/2024: The Level 2 TDISK version 05 and Level 2 ON2 version 04 data products have both been updated to revision 02. The only differences between revision 01 and revision 02 are the background values in the TDISK product and small changes to timestamps in both TDISK and ON2. No other variables including retrieved disk temperatures or derived $\Sigma O/N_2$ are impacted by the changes. It is not necessary for users to replace revision 01 with revision 02 unless users are specifically interested in the variables impacted. See sections 2.2.4 and 2.2.5 for details.

Update 9/13/2024: The Level 2 NMAX data product has been updated to version 04. The only difference between version 03 and version 04 are the values of the statistical (random) uncertainties in the retrieved peak electron density (the NMAX_UNC_RAN variable). See section 2.2.6 for details.

2.1 Level 1

2.1.1 Use of Ground Receipt Time in L1A Processing

Due to the large swings in temperature that the instrument experiences, the instrument clock drift is difficult to predict and correct for on the ground. The result is that the time error from using the instrument clock can be a significant source of error in the occultation measurements. This has been mitigated by tagging data packets with the packet ground receipt time minus the 130ms one-way light time from the spacecraft to the ground station. This is done using a metadata file generated on the ground that contains the ground receipt time of each packet. This file is used to assign UTC time stamps to each packet worth of data contained in each L1A file. The NAIF SPICE library is used to convert the UTC timestamps to the Ephemeris Time (ET) reported in the L1A files. The ground receipt time needed to perform this correction is not available for days prior to January 30, 2019, and data prior to that date will still exhibit timing errors.

There are two major effects that this change of time determination has on the data. First is that the timestamp in product filenames may change. This predominantly affects L1A and L1B products but can affect L1C and L2 products in cases where the time change caused the product start time to cross a minute boundary. Secondly, significant changes may be present in L1B and L1C geometry fields associated with occultation star location due to the sensitivity to timing errors.

2.1.2 Time-Dependent Filtering of Photon Events by Pulse Height

The GOLD detectors employ a z-stack of microchannel plates that convert single photoelectrons produced at their respective spectrograph focal planes into pulses with a gain of $\sim 10^7$ electrons

that are detected by their electronics packages (McClintock et al., 2020a and 2020b). The size of the pulse, referred to here as 'pulse height', is recorded by the electronics for each detected photoevent. It has been shown that the filtering of energetic-particle-produced events, which typically have higher pulse height values than events produced by photons results in a reduction of mislocated events that tend to cause a horizontal stripe across the detector when high particle backgrounds are present. McClintock et al. 2020a describe the particle backgrounds distributions and morphologies.

A nominal filter window was selected to filter out all events with a pulse height value of 0, 1, 2 or greater than 200. During the period 2020/345 to 2021/046, the Channel A detector was being run at very high gain due to advanced degradation at the 135.6 nm line. As a result, the pulse heights of normal photon events were increased significantly, and the pulse heights of ~20% of normal photon events were shifted beyond the nominal filter level of 200. To ensure that these normal photon events are not excluded, this release added the ability to adjust the pulse height filter window for each day. For the period of time when Channel A was being run at very high gain, the filter is configured to filter out events with pulse height values of 0, 1, 2, or greater than 250.

2.1.3 Improved Time-Dependent Background Subtraction

In the latest data release, two bugs have been fixed in the time-dependent background subtraction. The first update is that the area on the detector used to determine the background count rate has been adjusted to exclude detector rows that would occasionally see signal from a bright star located at the edge of the slit. This fixes a few L1C products where an erroneously large particle background was subtracted at an isolated East/West location. Figure 2-1 shows L1D before (left) and after (right) images from an affected observation.
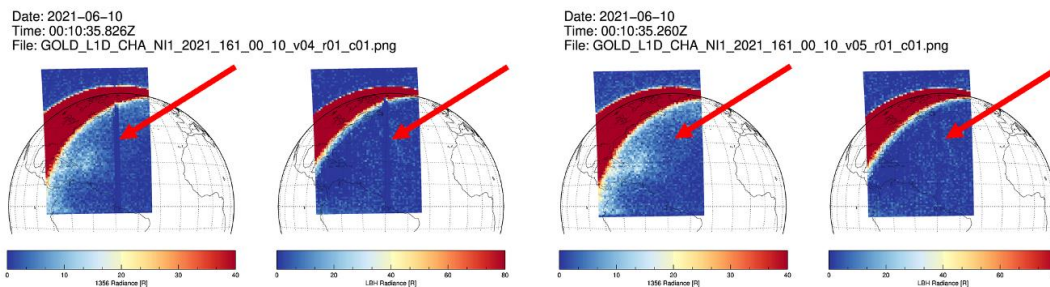
Figure 2-1 L1D images showing correction of background subtraction artifact

The second update fixes a fitting issue affecting the shape of the particle background image which is scaled by e background count rate. The extreme degradation caused by the presence of the Oxygen 130.4nm emission on the CHA detector was causing a bad background fit that imparted an incorrect background shape to the L1C data during times of high particle background. Figure 2-2 shows an example spectrum with the artifact introduced by this bug (top) as well as the same data with the artifact removed by the bugfix (bottom).
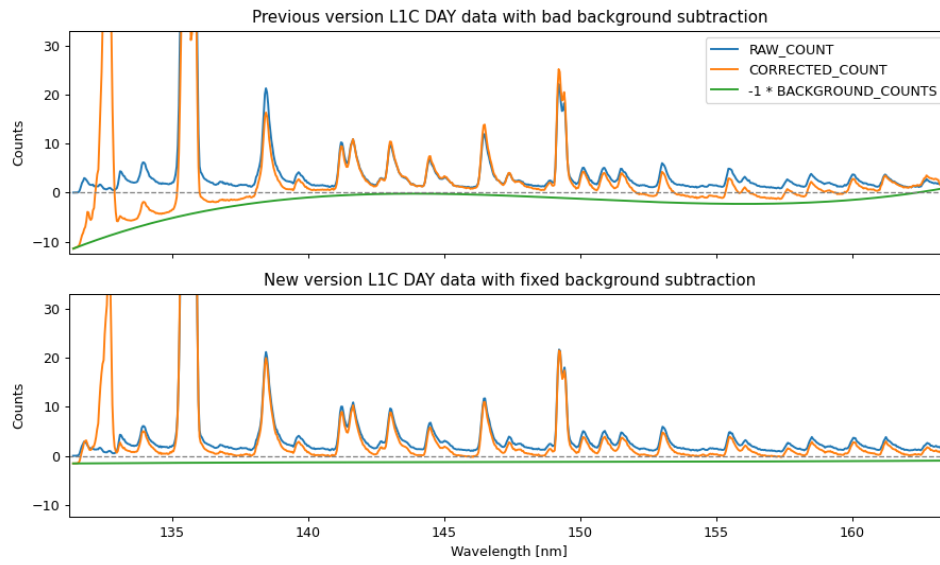
Figure 2-2 Spectrum showing correction of background subtraction artifact

2.1.4 Improved Geolocation

GOLD has performed three special pointing and alignment experiments where both channels pointed off either side of the disk and allowed a group of stars to drift through the field of view. These experiments were performed on 2018-285, 2020-267, and 2020-363. After analysis of these datasets, three changes were made to the GOLD calibration to improve the accuracy of derived geometry. The Channel A geometric correction calibration file was updated, the north/south tilt of the scan mirror was adjusted in the SPICE instrument kernel, and the definition of what rows of the detector the slit illuminates was adjusted. These combined changes minimized the pointing errors derived from the special pointing and alignment experiments. The resulting pointing errors are shown in Figure 2-3.

Figure 2-3 Pointing errors by GOLD channel

2.1.5 Improved High Particle Background Flag

The flag indicating the presence of high particle background levels during an observation stored in the global attribute named "High_Background" in DAY, LIM, DLM, and NI1 L1C files is now set based on a particle background count rate threshold of 0.01 counts/L1B pixel/second.

2.1.6 Improved Flatfield Correction

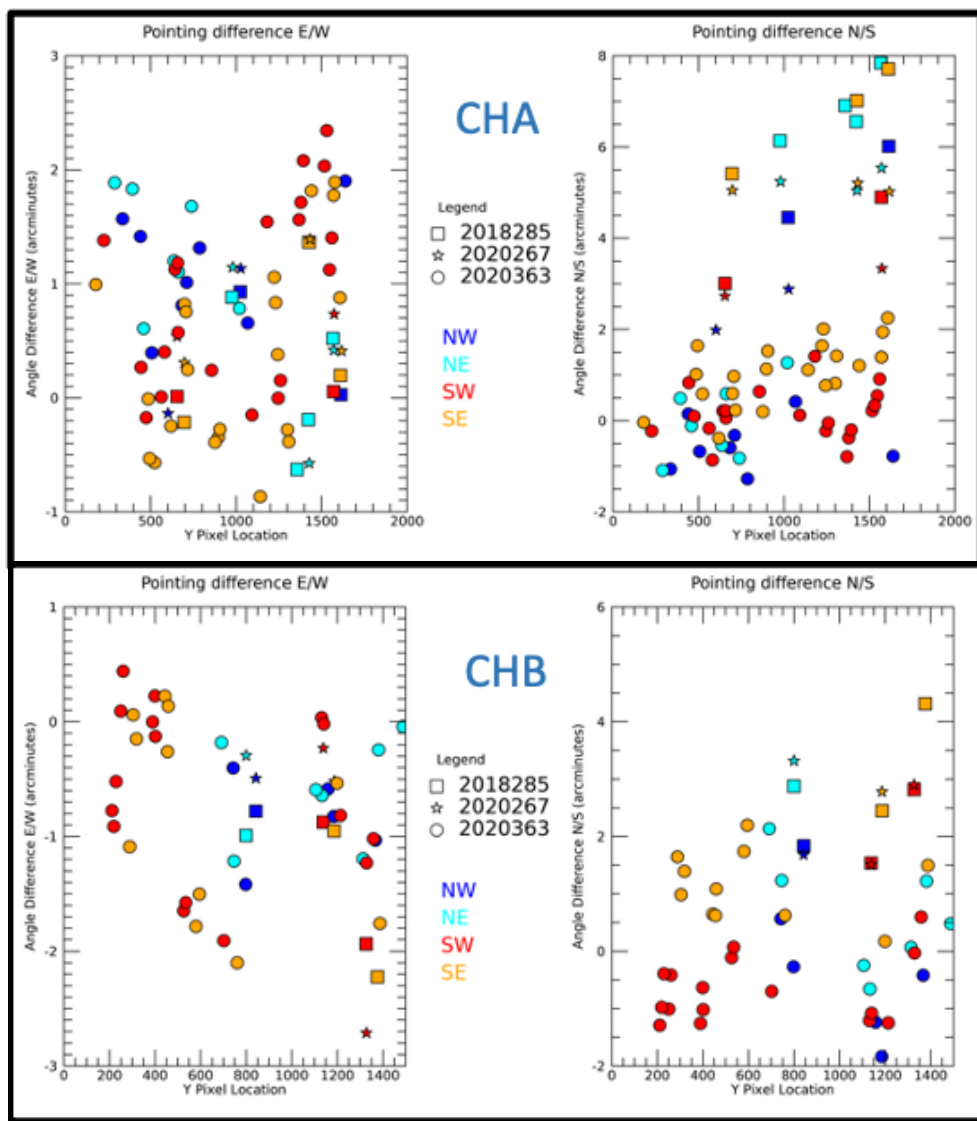The previous version L1C products contain data processing artifacts introduced by the flatfield correction algorithm. The previous algorithm failed to account for the change in the distribution of light on the detector from the flatfield lamp as a function of grating yaw mechanism (GYM) position (see section 3.1.1). The result was an erroneous reduction in the O 135.6 nm brightness of approximately 7% per year for the mission to date. In this release, the flatfield correction algorithm has been modified to remove this systematic error and make additional, overall improvements to the correction. The estimated change in overall band brightness resulting from these changes for Channel A can be seen in Figure 2-4.
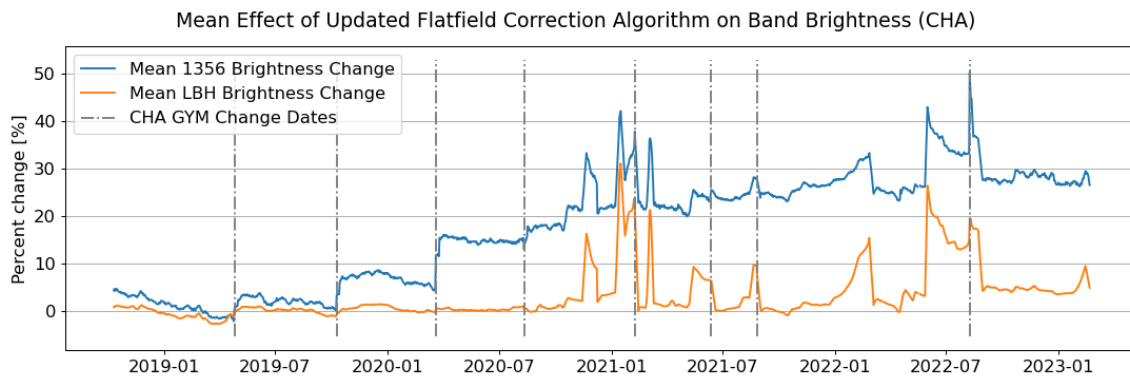
Figure 2-4 Effect of updated flatfield correction on band brightness

2.1.7 Added L1C Quality Flag Indicating Large Flatfield Corrections

L1C quality flags have been added to identify when flatfield corrections are large and data should be used with caution due to high uncertainty in the correction. To determine the quality flags, the applied flatfield correction is run through a forward model that estimates the change in O135.6 nm and LBH integrated brightnesses as a result of the correction. The resulting quality flag array is a row-dependent vector at L1B pixel resolution which is then binned to L1C resolution and stored in the Quality_Flag variable. It should be noted that the Quality_Flag variable contains bitwise flags which can be deciphered using the bitwise definition table in Section 4.6 of the GOLD Public Science Data Products Guide.

2.1.8 Added New Dark Limb Observation Type (DLM)

A new observation type has been added for observations of the night-side limb or Dark Limb (DLM). These observations were added to regular operations in order to observe the equatorial

ionization anomaly (EIA). They are identical to the standard limb scans (LIM) except that the distance scanned has been increased in order to cover a larger latitudinal range on the limb. This change also required that L1C processing be customized for DLM scans to cover the increased latitudinal range. DLM products also have a custom L1D quicklook which only shows the O 135.6nm emission brightness with an adaptive color scale to aid users in identifying the presence and structure of the EIA. See section 4.8 of the GOLD Public Science Data Products Guide for additional details.

2.1.9 Improved Background Subtraction for Occultations

The original airglow background subtraction implemented in L1C processing was developed during a time of solar minimum and an absence of EIA signal in night-side occultation data. As the sun became more active, it resulted in the regular presence of EIA signal in night-side occultation data, the GOLD team became aware that the airglow background subtraction algorithm in L1C processing of occultation observations did not handle the presence of EIA correctly. In this data release, the algorithm has been adapted to correctly identify and remove the EIA airglow from the stellar signal. In addition, a more thorough analysis was performed to characterize the solar zenith angle cutoff between day-side and night-side occultations. The result is that users can expect to see greatly improved occultation data for night-side occultations when the EIA was present and an improvement in the signal-to-noise ratio in occultations with a solar zenith angle with respect to the observed star between 95 and 110 degrees.

2.1.10 Corrected Calculation of L1C Systematic Uncertainties

In the previous version of the L1C data, a known issue was that the values for the radiance_systematic_unc underreported the magnitude of the uncertainty. This issue has been fixed in this release.

2.1.11 Fixed Occultation Metadata

The following global attributes present in the Level 1C occultation data products are now populated with correct values: SC_Alt, SC_Pos, SC_Z_Dir, SC_Nadir_lat, SC_Nadir_lon, SC_Yaw.

2.2 Level 2

2.2.1 Use of updated L1C data products

All L2 data products have been reprocessed from the updated L1C data. This produces an updated version number for all products whether or not the Level 2 algorithms for each product have changed since the previous version. The improvements in L1C processing described in section 2.1 propagate through to the Level 2 products in different ways. In many cases these

improvements have helped to fix artifacts seen in previous versions of these products. For example, the timing corrections and improved occultation background subtraction discussed in sections 2.1.1 and 2.1.9, respectively, had a significant impact on the O2DEN product but no effect at all on the other L2 products. Changes to the GOLD instrument calibration incorporated in this reprocessing result in an overall increase in the L1C spectral radiances, primarily at short wavelengths, as described in section 2.1.6. This change had a significant impact on those L2 data products that depend directly on the absolute oxygen 1356 radiance, specifically ON2, QEUV and NMAX. Other L1C changes, including improved background subtractions in the DAY and LIM L1C radiances and instrument calibration improvements in the long-wavelength (N_2 LBH) part of the spectrum, affected the TDISK and TLIMB temperature products.

All Level 2 data in the current release other than NMAX are derived from Level 1C Channel A data only. Both Channel A and B NI1 L1C data are used to derive the NMAX data product.

2.2.2 NMAX – assumed scale height; array size

The assumed scale height (H) used in the NMAX algorithm for the Chapman profile parameterization of the electron density profile has been updated. Previous versions used a value of 100 km for this parameter, whereas the new version assumes a 50 km scale height. The original value for the Chapman scale height was based on erroneous assumptions. The updated value is based on the typical scale height for atomic oxygen and shows good agreement with COSMIC Global Ionospheric Specification electron density profiles. Since NMAX is inversely proportional to the square root of H this change introduced a constant increase of ~1.414 in the v03 NMAX product relative to v02 (this increase is modulated by the changes attributable to updated L1C data).

Finally, all NMAX files will now have the same array size in the longitude direction. Since the scan range of NI1 observations (from which NMAX is derived) varies, arrays are padded with fill values to achieve the desired size.

2.2.3 Data Quality Index (DQI)

For this release ON2 and QEUV DQIs are now treated bitwise, bringing them into line with the treatment of DQIs for the other Level 2 data products. In addition, some DQI information is now incorporated from Level 1C data. Specifically, DQI bits for large 1356 flat field correction and large LBH flat field correction are set for all L2 data except O2DEN. In addition, a HIGH_BACKGROUND global attribute is carried over from L1C for all L2 types except O2DEN. Refer to the GOLD Public Science Data Product Guide for further information on Level 2 DQIs.

2.2.4   Time changes in revision 02 of TDISK v05 and ON2 v04 **(4/10/2024)**

The code used to bin Level 1C data before ingestion by Level 2 algorithms has been refactored, resulting in a more accurate method of combining timestamps. The impact of this change is a 1-second shift in some pixel level timestamps, as well as changes in the SCAN_START_TIME and SCAN_STOP_TIME arrays on the order of about 10 seconds for most cases, with a few cases of larger differences on the order of 1-5 minutes (mainly due to data gaps). The SCAN_START_TIME and SCAN_STOP_TIME arrays are provided as a convenience to the end user and now better reflect the time range of usable Level 2 data. This change does not affect any other variables, and it is not necessary to replace revision 01 with revision 02 unless a user is specifically interested in the changes to the pixel level timestamps or SCAN_START_TIME and SCAN_STOP_TIME variables.

2.2.5   Corrected background values in revision 02 of TDISK v05 **(4/10/2024)**

The values of the BACKGROUND variable were incorrect in revision 01 of the L2 TDISK v05 product. This error only affected the background values written to the netCDF files and did not affect any other variables, including retrieved disk temperatures. This has been corrected in revision 02 of the TDISK v05 product. It is not necessary to replace revision 01 with revision 02 unless a user is specifically interested in the BACKGROUND variable values.

2.2.6   Corrected statistical (random) uncertainties in NMAX v04 **(9/13/2024)**

An error in the calculation of the statistical (random) uncertainties in the retrieved peak electron density has been corrected in v04 of the NMAX data product. Prior versions of NMAX had incorrect values for the NMAX_UNC_RAN variable due to an emission angle not being converted to radians in a single term of a more complicated expression. The resulting change in the magnitude of the uncertainty varies with emission angle. In general, the statistical uncertainties will be smaller in NMAX v04 than in previous versions. No other variables in the NMAX product were impacted by this change.

2.2.7 Summary of changes in Level 2 data products

The GOLD Level 2 data products reprocessed for this release differ from the previous data versions to various degrees, depending on their sensitivity to underlying L1C changes and whether the L2 algorithms have changed. This section provides a high-level summary of the changes that users can expect to see in each L2 data product.

ON2:

The v04 ON2 is systematically higher than v03 due to the effect of the new L1C flat field correction on the absolute radiances used in the L2 algorithm. This is primarily driven by a large, time-dependent increase on the oxygen 135.6 nm radiance, and to a much lesser extent by

changes in N_2 LBH radiances (see section 2.1.6). Figure 2-5 shows a comparison of v04 (red) and v03 (blue) daily average ON2 in the Northern Hemisphere (left) and Southern Hemisphere (right). The top panel shows both data versions overplotted while the bottom panel shows the difference, in %. Vertical lines indicate the times of GYM shifts (see section 3.1.1). While the v03 data was characterized by a long-term downward trend, this artifact has clearly been removed in the reprocessing using the corrected L1C radiance data. Differences between the two versions grow from ~0 at the beginning of the mission to 40% or more by 2023. This closely mimics the changes in 1356 radiance shown in section 2.1.6.
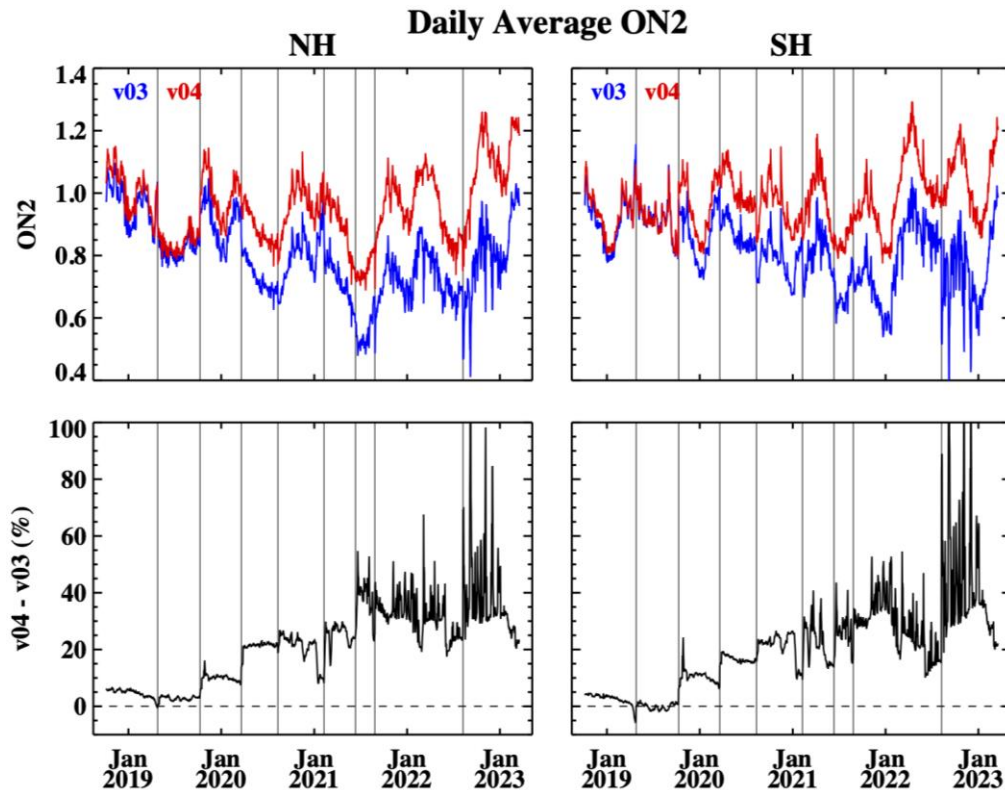

Figure 2-5 Comparison of v04 and v03 ON2 data

TDISK:

In general, changes in the new v05 TDISK data are small relative to v04. Figure 2-6 compares the daily average TDISK from both versions in the same format as Figure 2-5 figures (left panels show data from the northern hemisphere, right panels show data from the southern hemisphere, top panels are a direct comparison, bottom panels show the difference between the versions in %, vertical lines represent GYM shifts). Before ~ mid-2021 the mean differences in daily-average temperature are generally less than ~10 K, oscillating between positive and negative and generally resetting to zero at each GYM shift event.
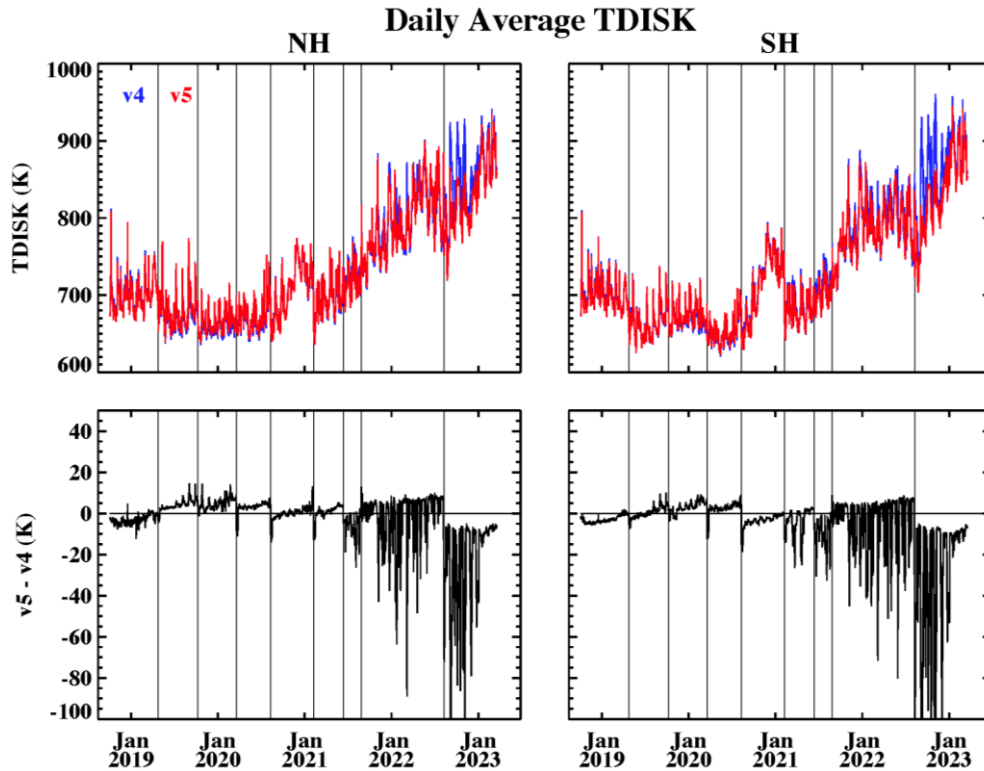
Figure 2-6 Comparison of v05 and v04 TDISK data

Beginning about the time of the 5th GYM shift event on February 8, 2021, we start to more frequently see large differences relative to the mean. These days of increasing v5-v4 difference are always negative, i.e., v05 is colder than v04. These larger, episodic divergences from v04 later in the mission can be traced to improvements in the L1C background removal algorithms for the dayside (DAY) disk data under conditions of high particle backgrounds at the satellite. After the 5th GYM shift, the bright 130.4 nm oxygen emission line began to appear on the GOLD detector and this feature introduced an artificial spectral curvature in the smoothed 2D background field subtracted from the DAY disk images (section 2.1.3).

The problem was exacerbated during times of high backgrounds, as illustrated in Figure 2-7. This figure shows the v04/v05 TDISK comparison during a 30-day period during September of 2022. As the top panel shows, the two versions agree very well at some times and diverge significantly at others (with v05 colder than v04 always). In the temperature difference plot in the bottom panel, the daily average background count level is overplotted in blue. Clearly the time periods where v05 diverges from v04 are highly correlated with increases in the background levels. During these periods, the v04 retrieval was biased hot due to unphysical curvature in the LBH spectrum caused by the incorrect background removal.
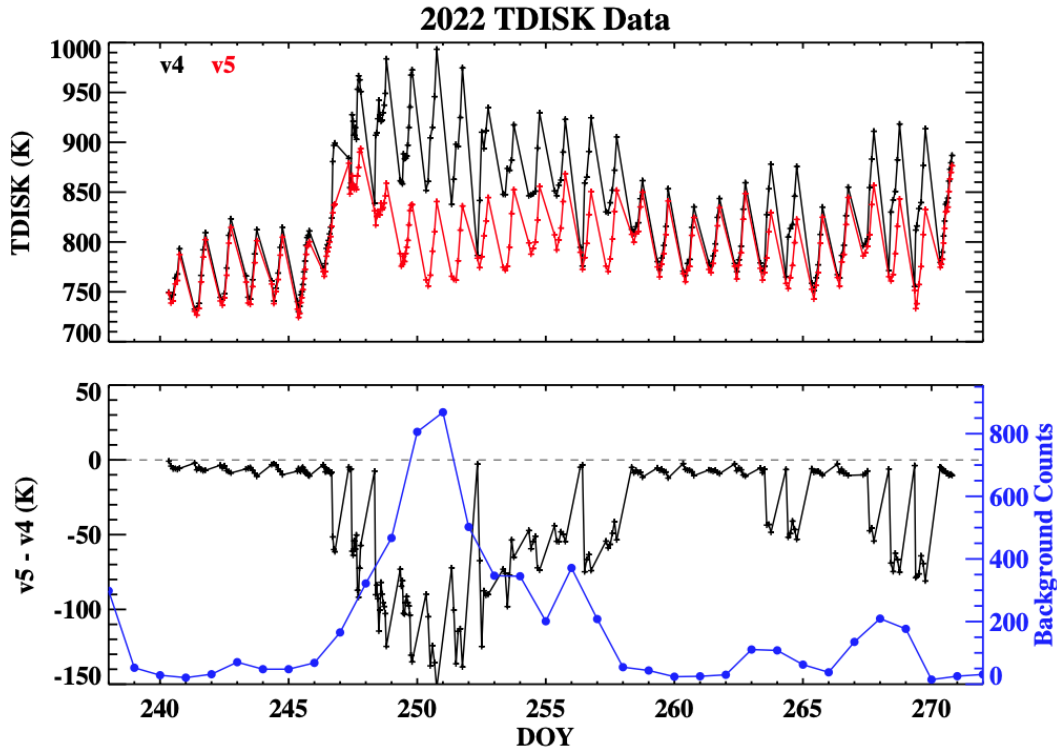
2022 TDISK Data

Figure 2-7 Comparison of v05 and v04 TDISK during September 2022

QEUV:

The v03 QEUV values are generally within ±5% of v02 through 2020. From 2021 through early 2023 there are times when the difference approaches 20% (v03 generally higher than v02). As with ON2, the change is primarily driven by changes in the L1C oxygen 1356 radiance due to improved flat field corrections. This sensitivity of QEUV to absolute 1356 is modulated relative to ON2 since it depends on a ratio of factors that partially cancel. Figure 2-8 shows the summary comparison of daily average v03 (red) and v02 (blue) QEUV, similar to the previous figures for the other L2 products (left panels show data from the northern hemisphere, right panels show data from the southern hemisphere, top panels are a direct comparison, bottom panels show the difference between the versions in %, vertical lines represent GYM shifts).

Figure 2-8 Comparison of v03 and v02 QEUV data

TLIMB:

There are minimal changes in v05 TLIMB compared to v04 with differences generally within 20K on average. Figure 2-9 shows the summary of daily average v05 and v04 TLIMB comparisons, similar to the previous figures for the other L2 products (left panels show data from the northern hemisphere, right panels show data from the southern hemisphere, top panels are a direct comparison, bottom panels show the difference between the versions in 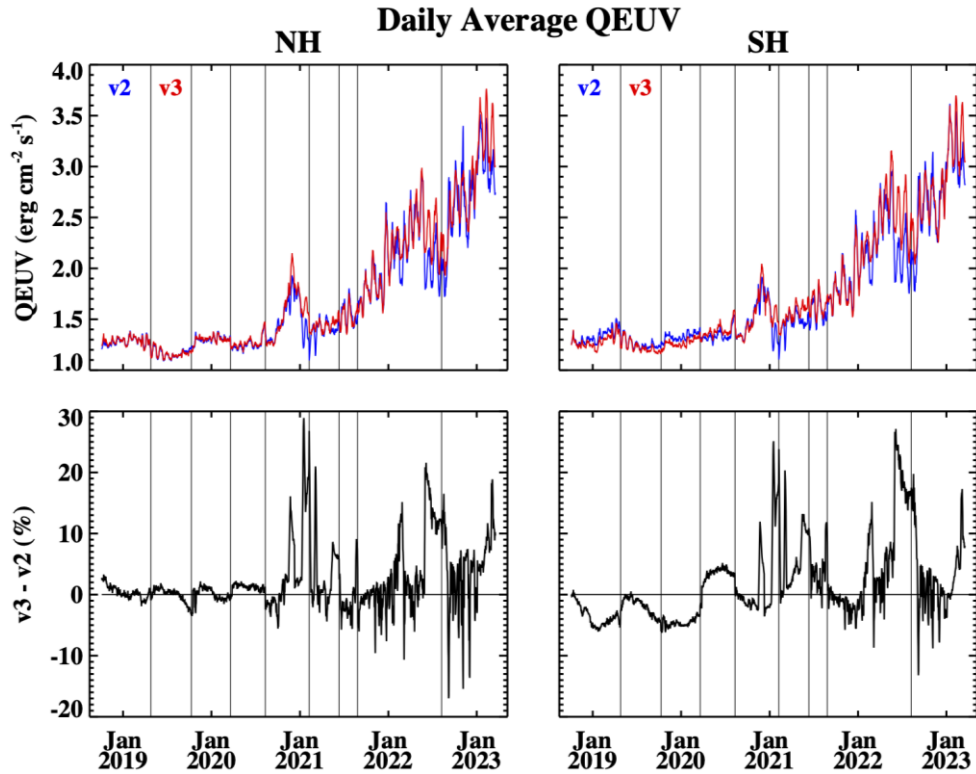%, vertical lines represent GYM shifts). Two features are noticeable in these plots. The first that the v05-v04 difference is of opposite sign in the two hemispheres – v05 is generally colder than v04 in the NH and warmer in the SH. The other feature is similar to that observed in the other L2 products, that the magnitude and variability of ΔTLIMB increases significantly starting in 2021. Daily average differences as high as 60 K occur in the NH in the first half of 2022.
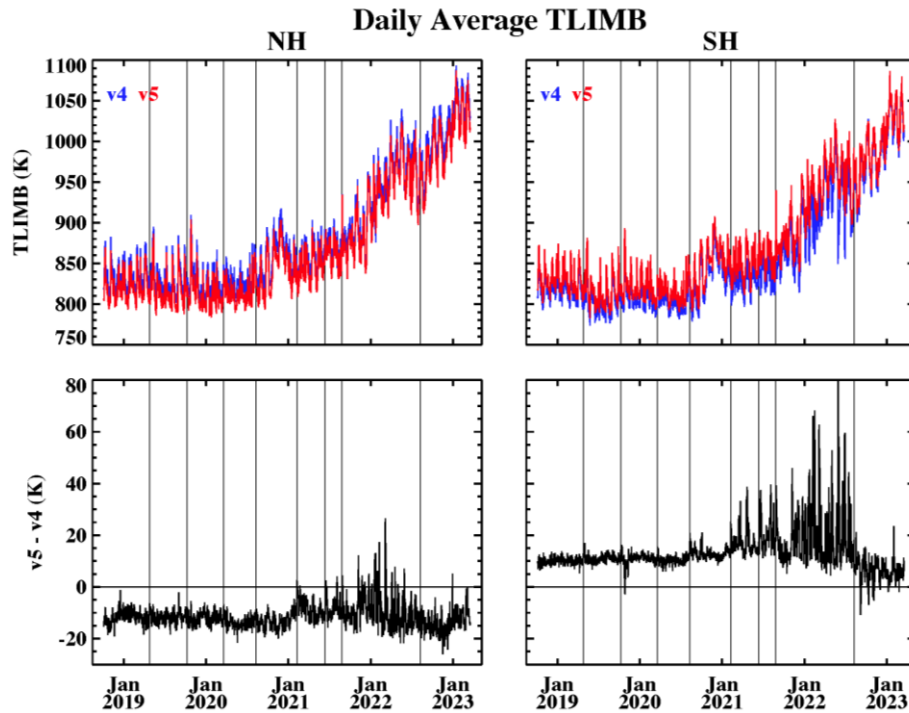
Figure 2-9 Comparison of v05 and v04 TLIMB data

As with the TDISK data, these periods of large differences in the new TLIMB data coincide with periods of high particle backgrounds. Figure 2-10 shows the ~1-year period between the 7th and 8th GYM shift operations, corresponding to August 2021 through August 2022. The TLIMB difference (ΔTLIMB , v05-v04) is overplotted with the particle background counts. The two quantities are obviously highly correlated, with large ΔTLIMB occurring on days with high backgrounds. This is reinforced by the results in Figure 2-11, which shows a scatterplot of ΔTLIMB vs the particle background counts over this same time period.

The explanation for this anomaly is essentially the same as for TDISK, discussed above. Improvements in the background removal algorithms for the L1C LIM limb data under conditions of high particle backgrounds at the satellite are responsible for this improvement. In the old L1C data version, during periods of high background the spectral artifact caused by the 1304 emission feature on the detector led to too much background being subtracted from the LBH limb profile at high attitudes. This flattened the profile (smaller apparent N2 scale height) and thus biased the v04 TLIMB temperatures low. This problem is fixed in the new reprocessed L1C data and the corresponding artifact in the v04 TLIMB retrievals does not appear in v05.

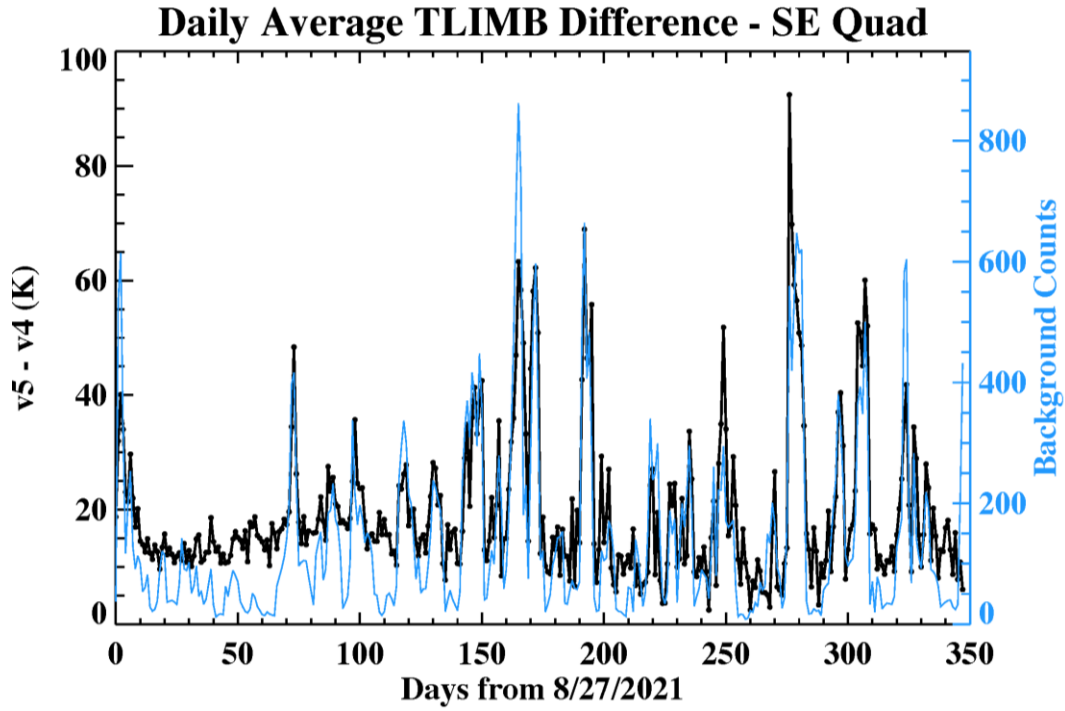**Daily Average TLIMB Difference - SE Quad**

Figure 2-10 Difference between v05 and v04 TLIMB for August 2021 – August 2022
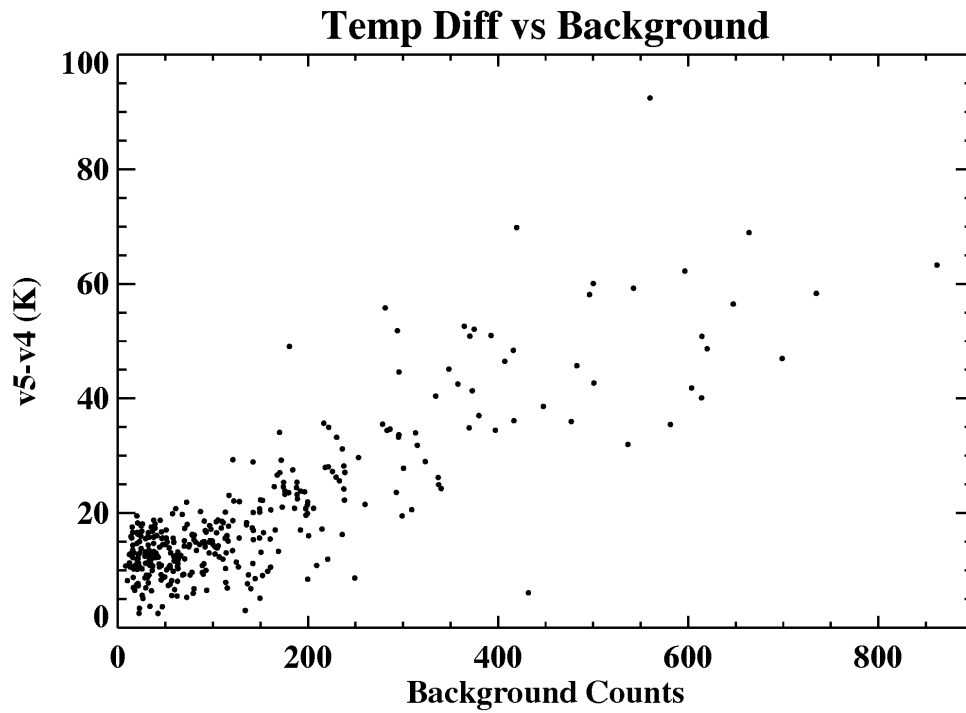
Temp Diff vs Background

Figure 2-11 Scatterplot of ΔTLIMB vs. background counts for the data shown in Figure 2-10

O2DEN:

There are significant changes in the v05 O2DEN dataset relative to v04. This is driven by two improvements made to the L1C OCC data. The most important improvement by far is the correction of timing errors in the Level 1 data time stamps described in section 2.1.1.

The instrument clock times previously used to timestamp the data were subject to large temperature-dependent drifts. The occultation (OCC) data is the only L1C data product that is highly sensitive to absolute timing, which is used to calculate the exact tangent altitude for the instrument line-of-sight to the setting or rising star. Timing errors in the old L1C OCC data could reach 5 seconds or more, resulting in altitude errors of up to 20 km. For a given absolute timing offset (positive or negative) the corresponding altitude errors would be of opposite sign for star rises (East limb) vs star sets (West limb). Altitude errors of this magnitude cause large biases in the retrieved O_2 density profile. Thanks to the correction of the timing errors in the L1C OCC data with this release, this issue has largely been eliminated (see section 3.2.1.5 for exceptions).

Further improvement in the v05 O2DEN data comes from the improved algorithms for background subtraction in the OCC data (see section 2.1.9). This primarily affects the nightside occultations.

Figure 2-12 shows a summary comparison of daily average v04 and v05 O2DEN for all nightside occultations (comparisons of the dayside occultations are similar). The v05 data (middle row) show significantly less scatter compared to v04 (top row). The differences (bottom row) show episodic large values, up to 100% or more, which are exactly correlated with the variation of errors in the instrument clock timestamps (not shown). These errors are alternately positive and negative and on average are roughly zero mean. This is consistent with the results in Figure 2-13, which shows profiles of the global mean difference and standard deviation over the entire data set. The mean difference is small, reaching a maximum of ~5% (v05 > v04) between 120 and 160 km. However, the standard deviation is large, peaking at 30%, indicating distribution of large differences.
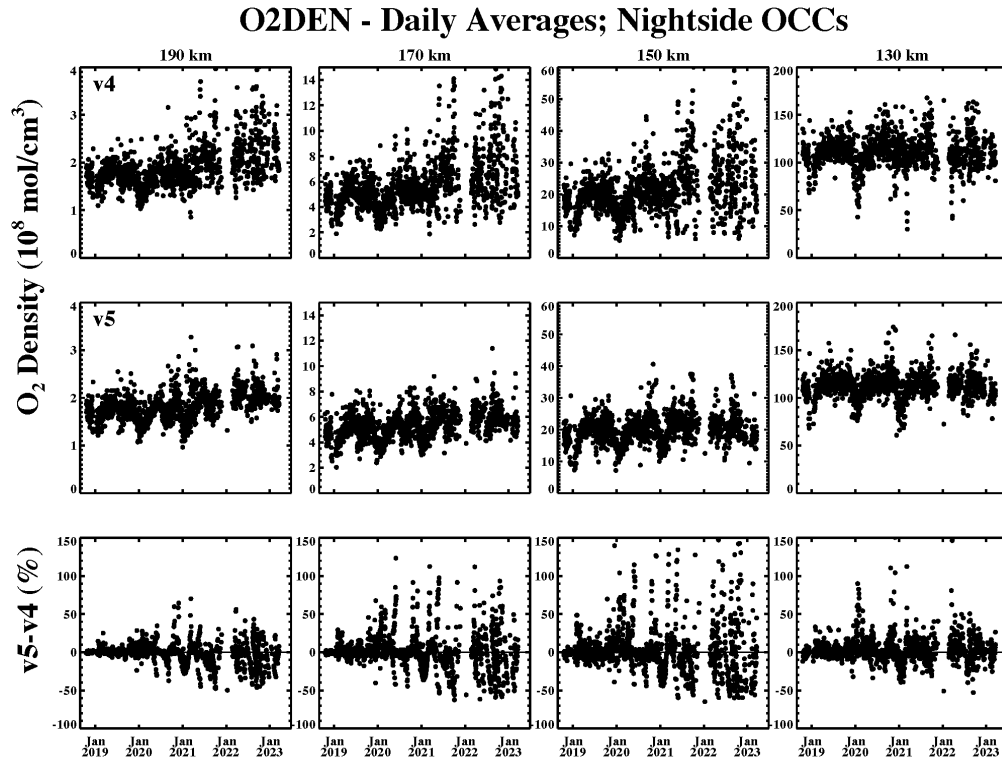
O2DEN - Daily Averages; Nightside OCCs

Figure 2-12 Daily average O2DEN data from nightside occultations at 4 altitudes (columns)

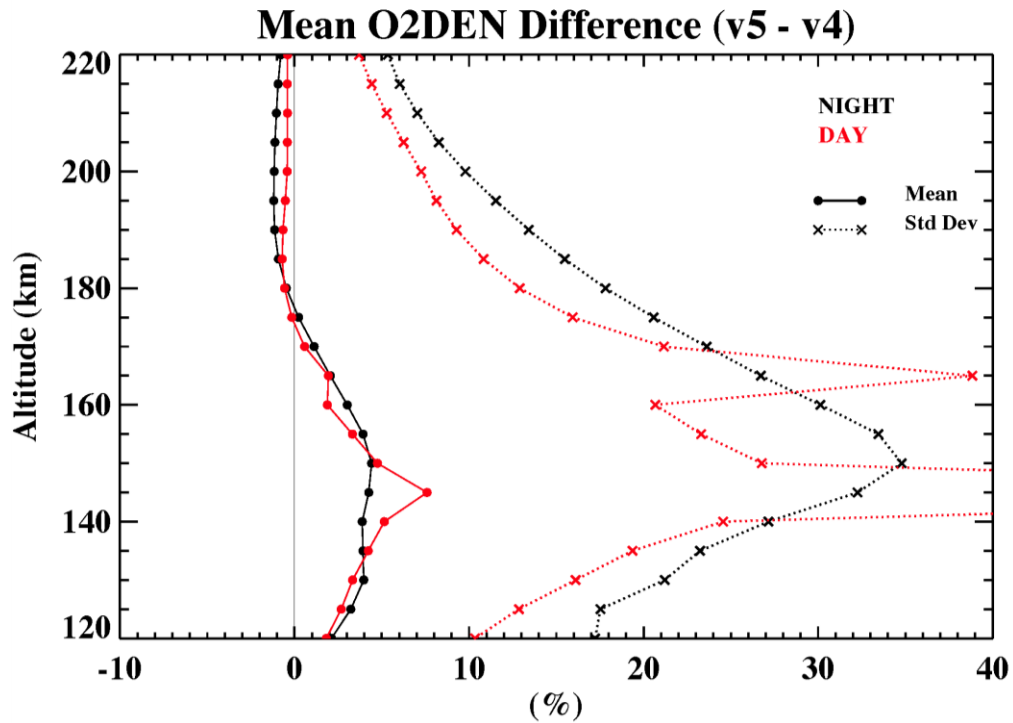## Mean O2DEN Difference (v5 - v4)

Figure 2-13 Global statistics for the v05-v04 O2DEN differences

NMAX:

The NMAX data is the only L2 product in this release that incorporates effects from both the changes in input L1C data as well as an L2 algorithm update. As discussed in section 2.2.2, the algorithm update consisted of a simple change in the assumed value of the electron density scale height, H, from 100 to 50 km. By itself, this change results in an increase in the v03 NMAX values by a constant factor of $\sqrt{2} \sim 1.414$ relative to v02.

The primary L1C change impacting NMAX is the effect of the new L1C flat field correction on the absolute radiances. As discussed previously, for Channel A this results in a large, time-dependent increase in the oxygen 135.6 nm radiance, growing to ~40% over the mission to date. Unlike all the other GOLD L2 data products, NMAX includes measurements from both GOLD instrument channels. The long-term calibration and degradation characteristics for the two GOLD channels are completely independent, however the changes in the reprocessed 1356 radiances from L1C Channel B are similar to what has been shown for Channel A. Since NMAX $\sim \sqrt{I_{1356}}$ this radiance increase transfers directly into the NMAX product.

Summary comparisons of daily average v03 and v02 NMAX for Channel A are shown in Figure 2-14, similar to the previous comparison figures for the other L2 products (left panels show data from the northern hemisphere, right panels show data from the southern hemisphere, top panels are a direct comparison, bottom panels show the difference between the versions in %, vertical lines represent GYM shifts). Similar comparisons for Channel B are shown in Figure 2-15,

The two separate effects described above are clear in both of these figures: the v03-v02 NMAX difference is consistent with an overall long-term increasing trend overlaid on the constant floor of a ~40% increase due to the algorithm change.

Update 9/13/2024: The NMAX data product has been updated to version 04, however this update only changed the random uncertainties in the retrieved NMAX values and not the NMAX values themselves. Therefore, the statements above regarding NMAX v03 also apply to v04.
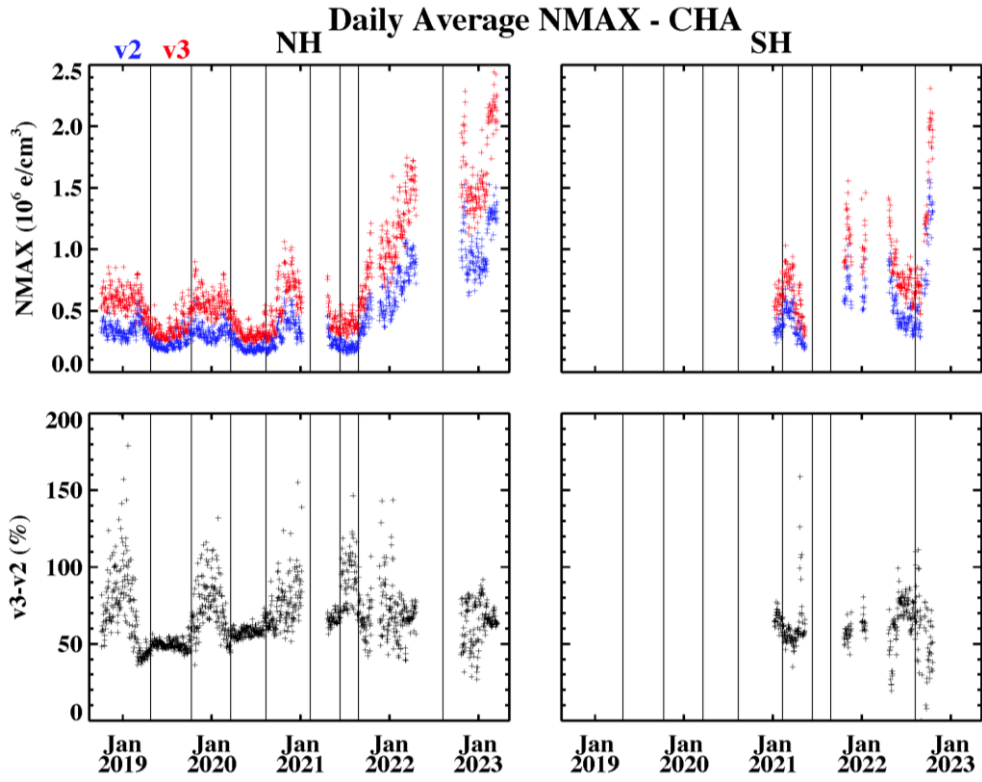
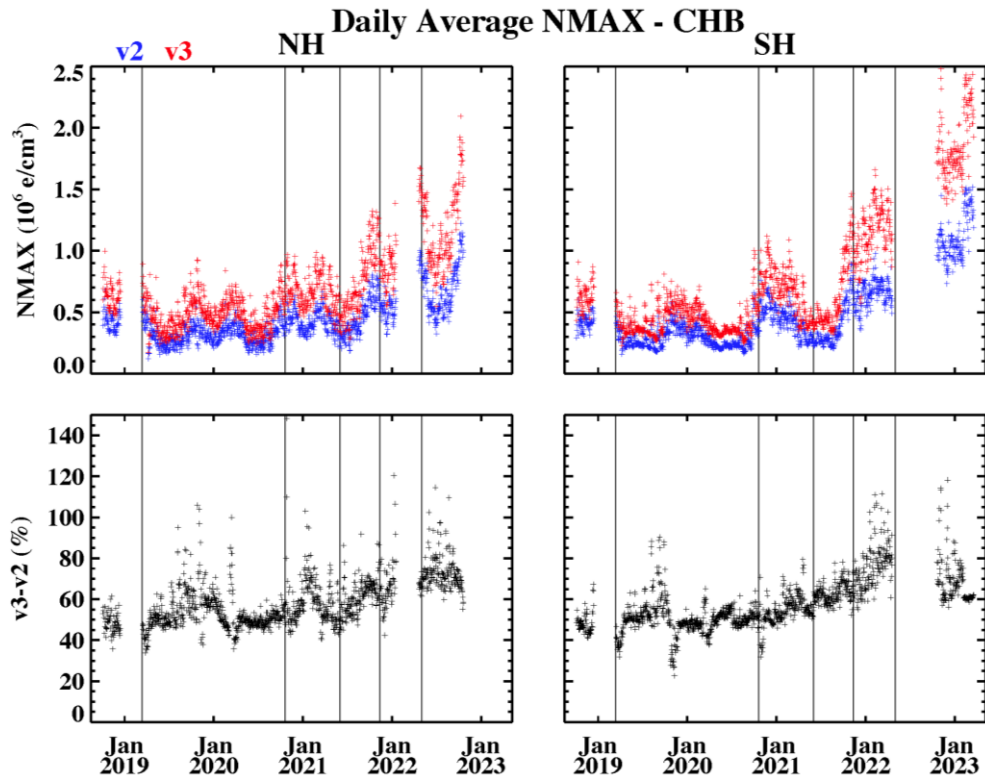**Figure 2-14 Comparison of v02 and v03 NMAX data (Channel A)**

Figure 2-15 Comparison of v02 and v03 NMAX data (Channel B)

3   Known issues:

There are a number of known issues with the data provided in this and previous releases. This section provides a description of these issues and guidance to the user community on the use and interpretation of GOLD data products. This documentation is cumulative so that descriptions of known issues will remain until they are resolved in future releases. For the current release, Section 3.1 describes known issues with Level 1 data while Section 3.2 describes known issues with the Level 2 data.

3.1   Level 1

3.1.1   Detector "burn-in"

The GOLD detectors employ a z-stack of microchannel plates that convert single photoelectrons produced at their respective spectrograph focal planes into pulses with a gain of ~ 10^7 electrons that are detected by their electronics packages (McClintock et al., 2020a and 2020b). The size of the pulse, referred to here as 'pulse height', is recorded by the electronics for each detected photoevent. As the detectors accumulate events, pulse height declines, a process that we refer to as 'burn-in'. This primarily affects emissions produced by the OI 135.6 nm doublet and is mitigated by using an internal stimulus lamp to obtain a 'flat field image' that is used to remove burn-in. As the gain continues to decline, errors introduced by the flat field process can become unacceptably large (as occurred during the first year of the mission). Before that point, a mechanism (Grating Yaw Mechanism – GYM) within the affected spectrograph is actuated to rotate the grating, placing the spectrum on a different location on the detector. At the beginning of the mission, the doublet was placed at the edge of each detector's active area. The GYM mechanisms have been actuated from time to time as summarized in Table 3-1. Each actuation moves the spectrum such that the OI 135.6 nm doublet is positioned on an undegraded region of the detector. All GYM moves, with the exception of the Channel A GYM moves in 2022 and 2023, have shifted the spectrum to longer wavelengths by approximately 0.8 nm (~ 20 L1C detector pixels). Because Channel B observes only during the night, the fluence of photons is much smaller than that for Channel A and its GYM has been actuated fewer times.

Detector GYM Actuation Dates	
Channel A	**Channel B**
4/26/2019	3/14/2019
10/10/2019	10/20/2020
3/20/2020	6/1/2021
8/11/2020	11/11/2021
2/8/2021	5/3/2022
6/12/2021	11/9/2022
8/27/2021	9/20/2023
8/9/2022	
5/30/2023	
11/7/2023	
12/11/2023	
4/22/2024	

Table 3-1 Detector GYM Actuation Dates

Daytime airglow emissions are the dominant contributor to the total fluence of 135.6 nm photons and therefore to sensitivity decline at 135.6 nm. Because the useful range of motion for the GYM is limited, the cadence of Channel A daytime observations was reduced beginning on 9/6/21 in order to extend production of the 135.6 nm-dependent Level 2 data products (NMAX, ON2, QEUV). In addition, stellar occultation observations are now being restricted to nightside occultations only.

3.1.2 Gradient in sensitivity from top to bottom of detector

The Channel A instrument sensitivity varies over the field of view (along the spectrograph entrance slit). This effect can be as large as ~20% from top to bottom of the slit. This is corrected for by application of a 2-dimensional sensitivity function to Channel A data as a step in L1C processing. This correction has reduced the magnitude of this effect but has not eliminated it entirely. The left six panels in Figure 3-1 plot the percent difference (southern hemisphere – northern hemisphere) of 135.6 nm emissions at 6 UT scan times during the day over the course of the mission. These differences are calculated from data averaged in a 10° x 10° (latitude x longitude) bin centered at the equator and the sub-satellite longitude. Vertical blue lines mark the days when the grating GYM was actuated. Large differences for times after 12:00 LT, present just before the first two actuations and just after the second one, result from severe detector burn in that could not be adequately corrected by the flat field algorithm. Differences in total LBH emission are plotted in the right six panels. Although these plots show little evidence for detector-gain induced artifacts, there appears to be an overall ~ 10% decline that most likely results from residual errors in the 2-D sensitivity function for longer wavelengths. This trend is not observed in the 2-D sensitivity for OI 135.6nm.
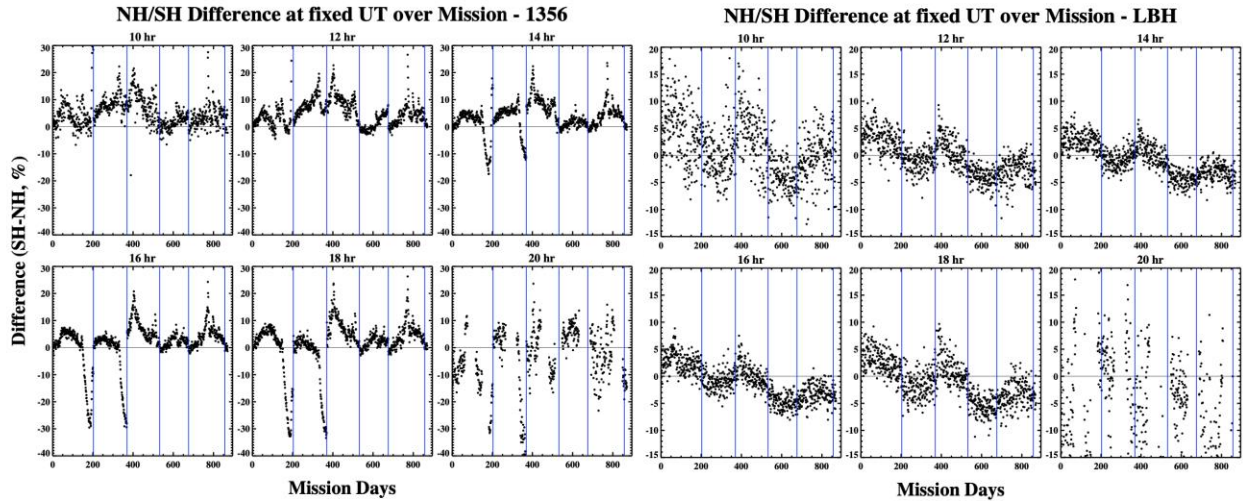
Figure 3-1 Percent differences (southern hemisphere – northern hemisphere) in OI 135.6nm (left six panels) and in total LBH (right six panels) for 6 times during the day throughout the mission.

3.1.3 Time Delay of Reconstructed Full Disk Images

The projected height of the slit covers slightly more than half the Earth, with an overlap around the equator when scanning the northern and the southern hemispheres. Not all banding observed in these overlapping scans is caused by residual errors in the instrument 2-dimensional sensitivity function (Section 3.1.2). Full disk images made by combining northern hemisphere radiance images with those from the adjacent (in time) southern hemisphere image, can also show banding because incidence and emission angles change throughout the 30 minutes during which the images are obtained. The effect is more pronounced early and late in the day. Figure 3-2 shows this effect on a sample DAY scan.
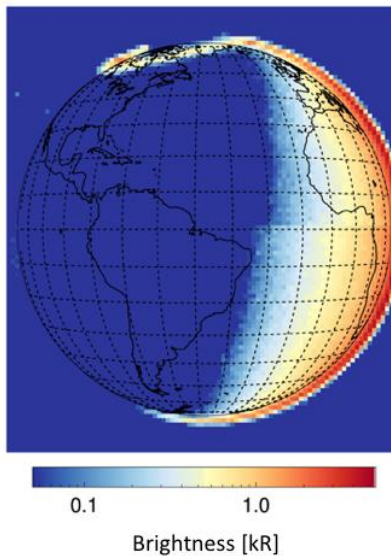

Figure 3-2 Combined scans of north and south latitudes from L1C data

3.1.4 Incomplete Scattered Light Correction

Due to the signal to noise limitations, the first version of the background and scattered light removal algorithm assumed that there is no wavelength dependence. This has not been corrected in the current release. Figure 3-3 shows that there is a small slope for regions of the spectrum < 138 nm that is not removed by the current processing.
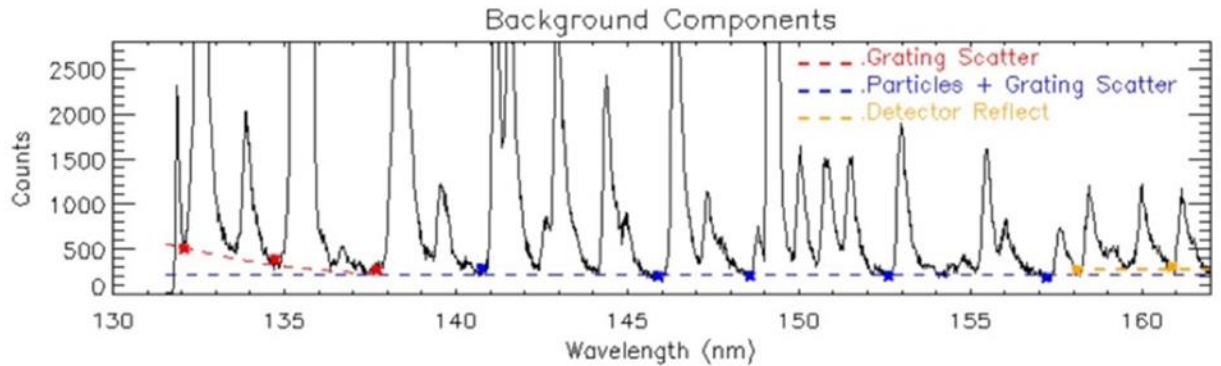

Figure 3-3 Wavelength Dependence Scattered Light

3.1.5 Flatfield Correction

The flatfield correction attempts to correct for a relative drop in detector sensitivity due to line burn-in. See the GOLD Public Science Data Products Guide (section 4.4.1.1) and McClintock et al., 2020b. The flatfield correction has some limitations. It is not always able to totally account for variations in detector gain that are caused by diurnal temperature variations in the instrument. The result is that the flatfield correction can under- or over-correct data, depending on the time of day and season. In addition, those parts of the slit that observe the aurora receive larger photon fluence and 'burn-in' more rapidly. These areas can be under-corrected. The error is largest for the brighter component of the 135.6 nm OI doublet and increases with 'burn-in', typically reaching maximum value just before a GYM actuation. This is particularly true for the first two GYM actuations (4/26/2019 and 10/10/2019). Figure 3-4 shows a simulation of the magnitude of the flatfield correction on the brightness of two emission features in the Channel A spectrum. These curves were produced by multiplying a model observed spectrum from the first days of the mission by the flat field images taken on the day of observation to produce a simulated spectrum with burn-in. The radiances extracted from the 'burn-in' images are then compared to those from the model observed spectrum to compute the magnitude of the correction for that day. Figure 3-5 shows the impact of the flat field correction errors on L1C DAY observations. An under-correction (left panel) of the 135.6 nm emission occurs for latitudes just south of the equator in a southern hemisphere scan approximately 1 month before a GYM actuation. This part of the slit observes the auroral region during northern hemisphere scans. Diurnal instrument temperature variations can sometimes result in an over-correction (right panel) of the 135.6 nm radiance.
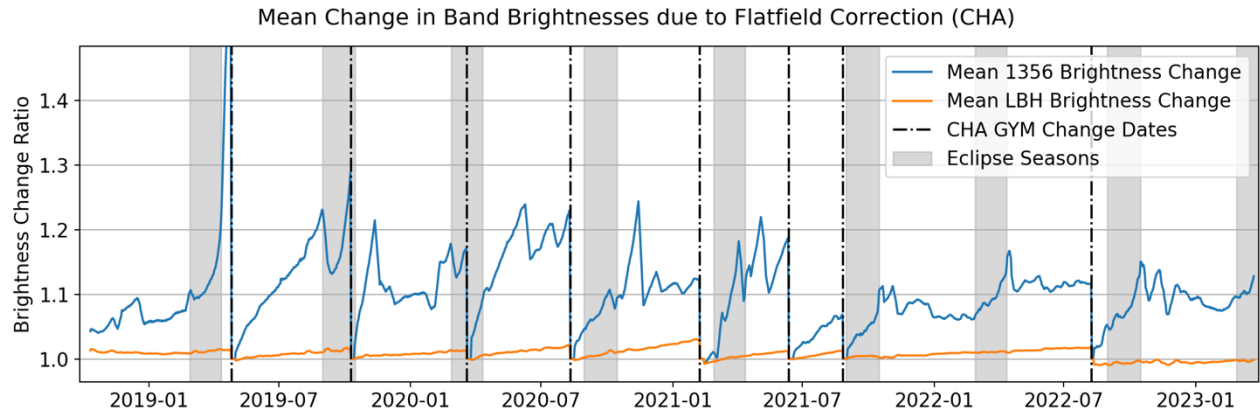
Figure 3-4 Channel A Expected Flatfield Correction. Vertical dashed lines and shaded areas denote GYM shift dates and period when the earth occults the sun during some part of a day.
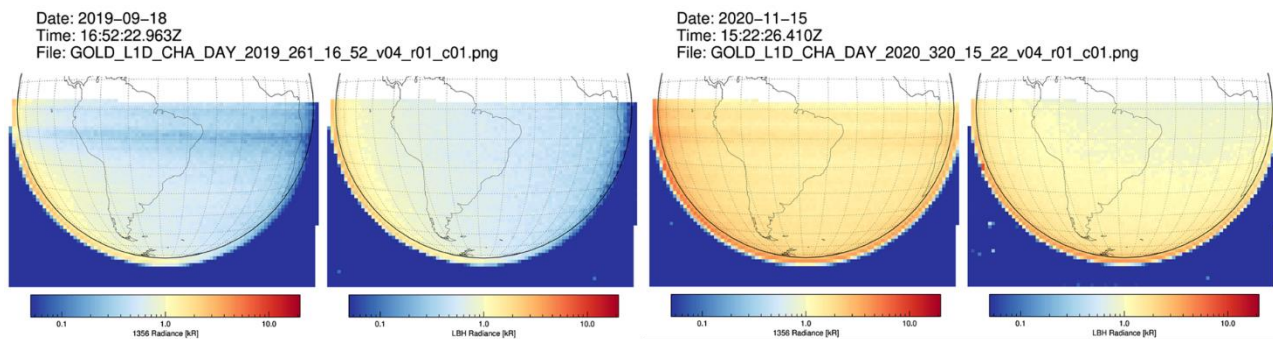

Figure 3-5 Effect of flat field correction errors on L1C DAY observations. The horizontal banding is the result of under-correction (left panel) or over-correction (right panel) of the 1356 radiance.

3.1.6 Limited Channel B Data

During the first three months of operations, the Channel B degradation (also referred to as 'burn-in') proceeded faster than expected. As a result, the 135.6 nm data became unreliable about December 15, 2018, but the GYM was not activated until March 15, 2019. Since then, the use of Channel B has been largely restricted to nighttime observations when the 135.6 nm emissions are an order of magnitude less than daytime emissions. As a result, the Channel B 135.6 nm radiance values reported after March 15, 2019 are reliable. Initial analysis of GOLD nighttime data from Channel B during December 15 of 2018 to March 15 of 2019 indicates that the current version of the data from that period are useful for qualitative analysis but not for quantitative analyses. To avoid unintentional inclusion of the unreliable radiances in quantitative analyses, the nighttime data for that period are not included in the .tar files generated in searches for data on the GOLD website. However, the data for that period is available by request through a link on the GOLD data download page (https://gold.cs.ucf.edu/search).

For Channel B, only nighttime (NI1) data is currently available. Channel B has made most of GOLD's nighttime observations, and release of Channel B nighttime data were given priority

over the Channel B daytime observations since Channel A provides the most comprehensive daytime coverage.

3.1.7 Slit Movement due to Thermal Changes

The projected image of the slit on the detector moves vertically ~ ± 2 L1B pixels with changing temperature throughout an orbit and throughout the year. We are currently using the "nominal" slit position on the detector to assign a latitude to every corresponding row along the slit and are not correcting for any movement of the image of the slit in that dimension (In contrast, the wavelength scale is determined from the position of the OI 136.6 nm doubles and NI 149.3 nm triplet atomic emissions for each L1C image). This effectively adds additional uncertainties in the assigned latitude. The image in Figure 3-6 traces the displacement of the bottom of the slit image relative to row 52 in each L1B spectral-spatial image as a function of universal time (UTC) and of season throughout a year. Typical range of motion throughout the day is ~ ±2 L1B pixels (~± 30 km in latitude at nadir) with comparable seasonal variation. This instrument effect will be corrected in a future release.
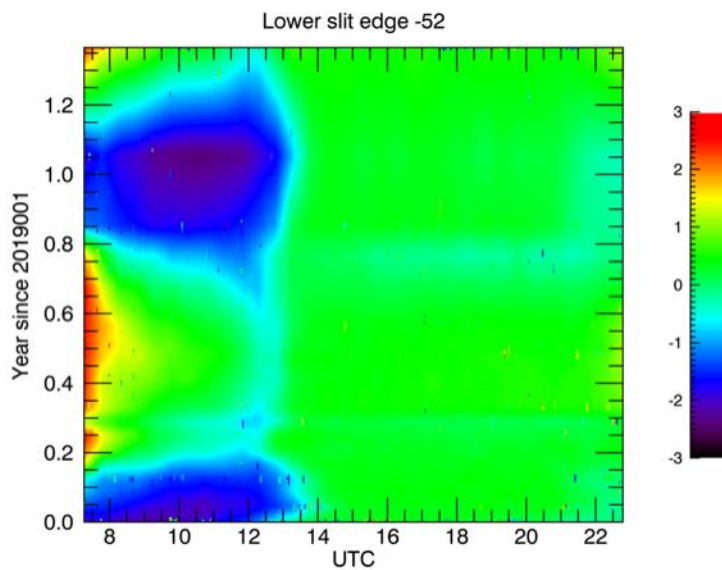
Figure 3-6 Vertical Slit Motion with Temperature measured in L1B pixels

3.1.8 Stellar Occultation Wavelength Feature

The wavelength determined during a stellar occultation is purely a function of the star within the occultation slit and so the solution is not applicable when the star is outside that field of view. For these time steps, the default high resolution slit wavelength solution is used. This adds an unrealistic discontinuity in the wavelength scale. This known displacement is present in this data release.

3.1.9 Incorrect Background Subtraction at Limb in Day Scans

The sharp transition in the background between On and Off Limb is not accurately captured, so the background is over corrected as seen in Figure 3-7. This will be addressed in future releases.
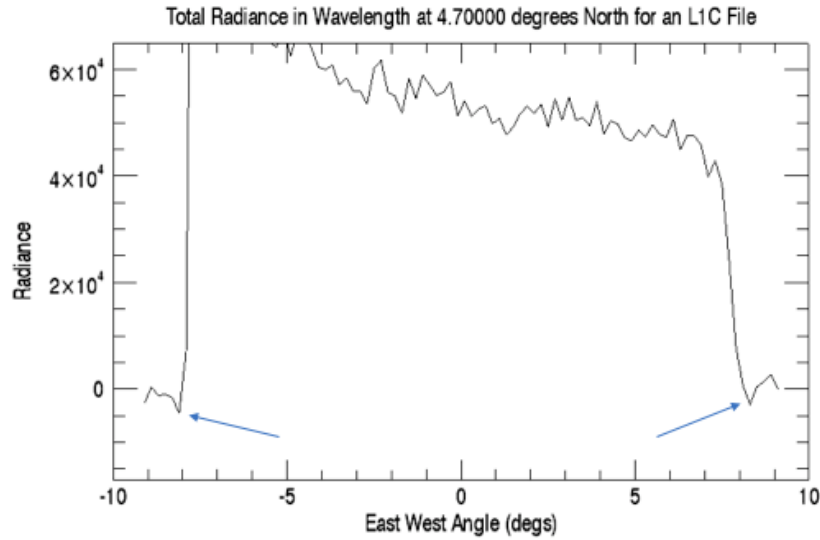

Figure 3-7 Over Corrected Background Subtraction at Limb

3.1.10 No local dead-time Correction for Occultations

Local dead-time correction, which affects the Occultations, has not been applied. The magnitude of the effect varies with the brightness of the star. A sample correction is shown in Figure 3-8.
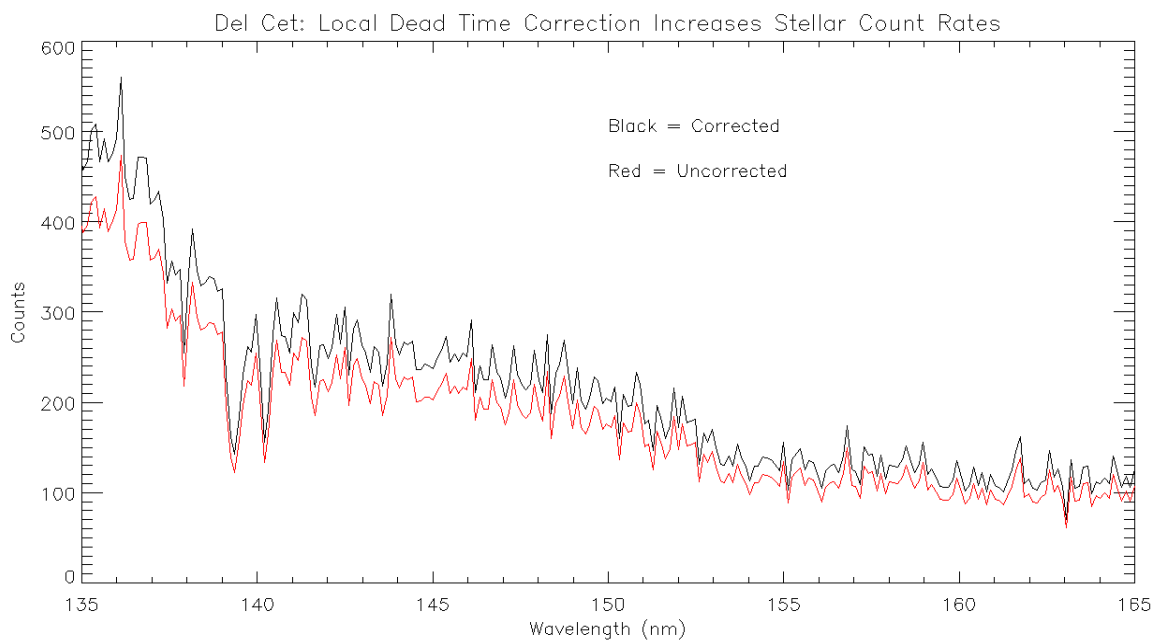

Figure 3-8 Counts Comparison with Dead-Time Correction

3.1.11 Variation in Spectral Resolution Along the Spectrograph Entrance Slit

The point spread function for GOLD spectra, which is well approximated by a Gaussian function, varies as a function of position along the slit and as a function of wavelength. Panels in Figure 3-9 are contour plots of PSF full-width-at-half-maximum (FWHM) for the southern hemisphere (rows 0 – 55) and northern hemisphere (rows 50 – 104) of L1C image cubes. PSF values are largest at the ends of the spectrograph entrance slit, which occurs for L1C row 55 in southern hemisphere scans (top of the spectrograph) and for L1C row 50 in northern hemisphere scans (bottom of the slit). Since the use of a single PSF for the entire slit in algorithms to retrieve temperature from LBH band shapes can introduce a latitude dependent bias to higher temperatures, a varying PSF is used for the retrievals.
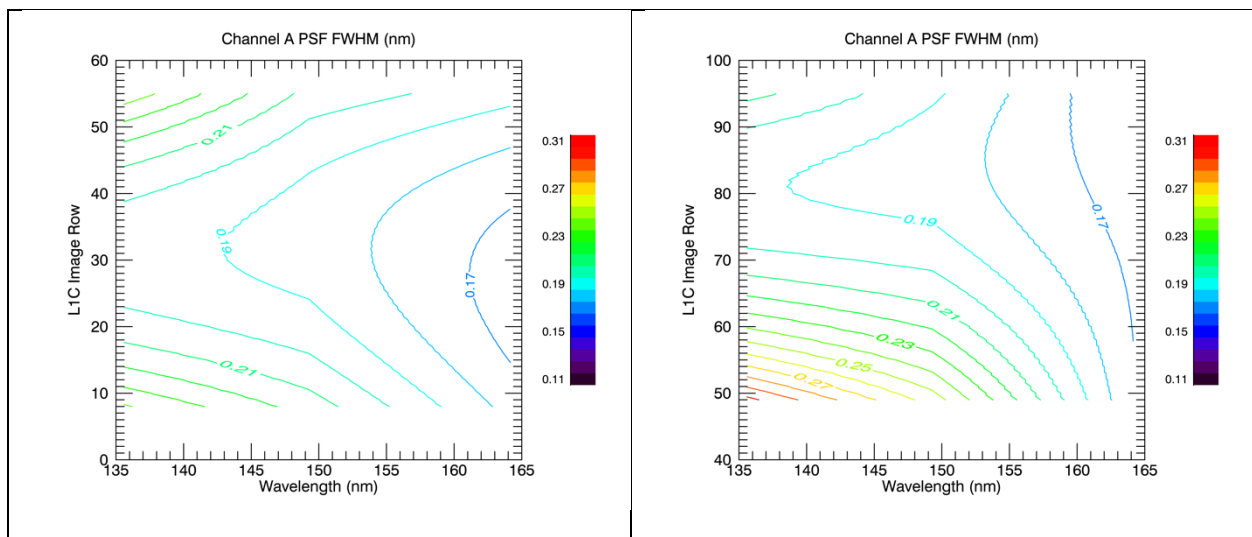

Figure 3-9 Contour plots of FWHM for GOLD's spectral point spread function

3.1.12 Errors in the L1C Wavelength Scale

A single wavelength scale is assigned to all spectra in an L1C image cube. It is calculated by coadding all the spectra in the cube to form a total spectrum and fitting the positions of the atomic lines of the OI 135.6 nm doublet and the NI 149.3 nm triplet to a linear function. (Early in the mission, an OI 164.13 nm was also used in the fit but is not now available since GYM actuations have moved it out of the spectrograph pass band after August 10, 2020).

Figure 3-10 compares the average wavelength scale solution to the solutions for the individual rows in an L1C data cube. The left panels are plots of the differences between the wavelength of pixel 0 (800-element (0 – 799)) in the scale fit to each row and the wavelength of pixel 0 in the scale fit to the spectrum of all spatial pixels. The top includes rows 8 – 55 (southern hemisphere L1C file) and the bottom includes rows 40 – 95 (northern hemisphere L1C file). These indicate that the starting wavelength in each row typically varies by less than 0.5 pixels (0.02 nm) over most of the L1C image cube. The right panels are plots of the differences between the total length of the wavelength range (typically 32 nm) for scale fit to each row and the scale fit to all

spatial pixels. These results are valid for wavelength scales derived by fitting 3 wavelengths (135.6, 143.9 and 164.13) or by fitting only the first two wavelengths. These results indicate that the single solution is accurate to better than ±1 pixel or better. Currently, researchers requiring better accuracy should use their own fitting routines.
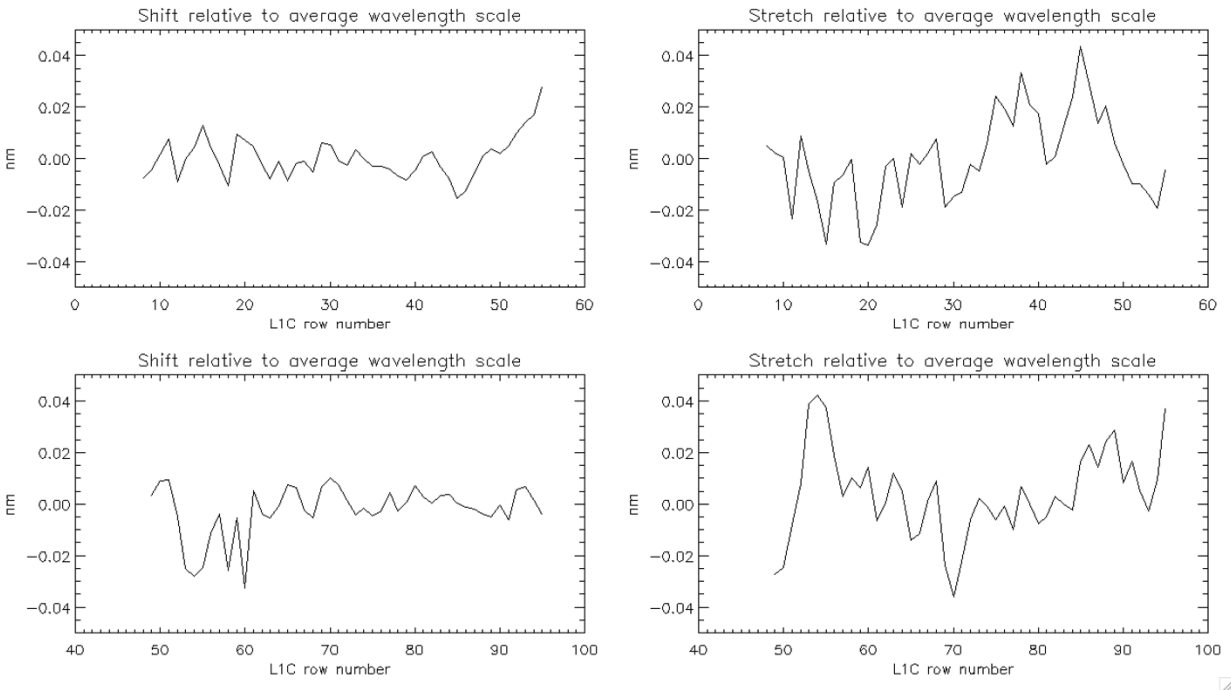
Figure 3-10 Wavelength scale shift-stretch for individual L1C image cube rows relative a wavelength scale for the entire

3.1.13 No Moon Flag

The presence of the Moon in the field of view is currently not being flagged during processing. This could affect the Limb and Occultation measurements. This issue will be addressed in future releases.

3.1.14 No Xenon Emission Flag

The SES-14 spacecraft that hosts the GOLD instrument uses ion propulsion for spacecraft station-keeping maneuvers. Its thrusters use xenon gas as a propellent, and it has been found that the GOLD instrument sees a xenon emission line at 146.96nm during these maneuvers. A quality flag that indicates the presence of this spectral feature will be added in a future release.

3.1.15 Noise due to High Particle Background

Particles from the radiation belt(s) produce counts in the detectors of GOLD and can appear as bright, noisy pixels when the particle background levels are high. Periods of high particle background are flagged in the L1C DAY, LIM, and NI1 data through the use of a global attribute named "High Background". Some examples of such noisy data are shown in Figure 3-11 and Figure 3-12.
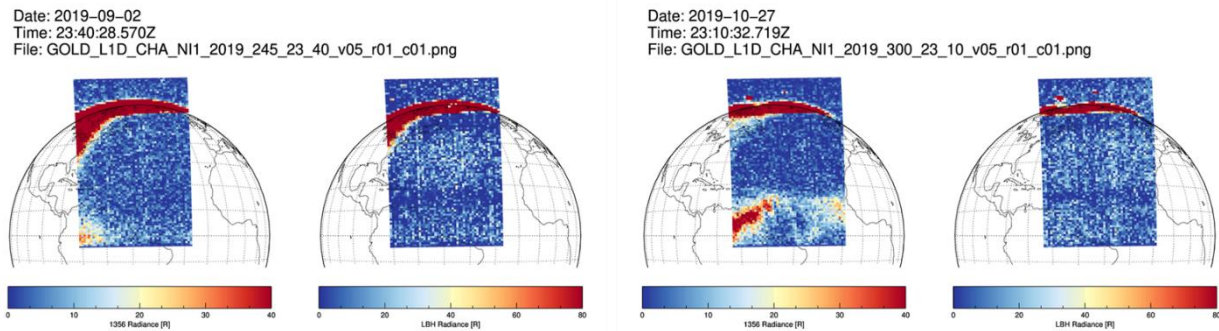
Figure 3-11 Examples of bright noisy pixels in night time images due to high particle background
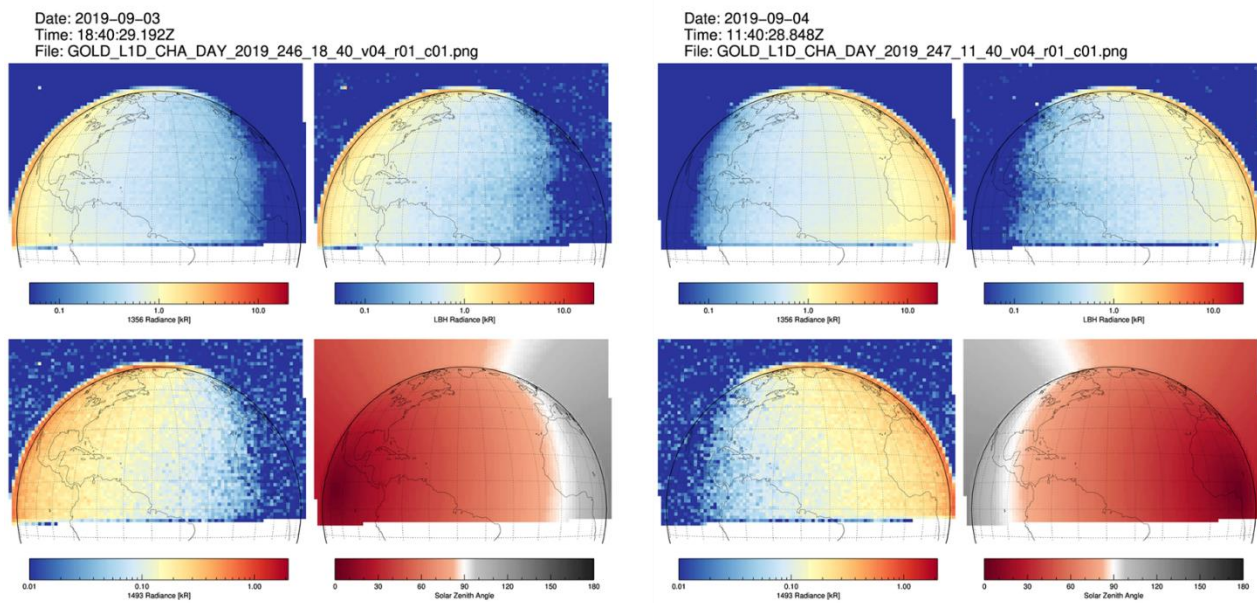
Figure 3-12 Noisy pixels in day time images due to high particle background; more prominent in the LBH emissions which have lower B(R) per pixel, but similar background per pixel

3.1.16 Field emission type events

Some anomalous events occur on the GOLD Channel A detector in both DAY and NI1 observations at LBH wavelengths. These events are most apparent in the night (NI1) images as seen in Figure 3-13. They appear at mid latitudes between 15° to 60°. These may be due to field emission events within the detector housing. Their position on the detector corresponds to

midlatitudes (vertically) and within the wavelength range of the LBH band emissions (horizontally). Such events are not flagged in the released data.
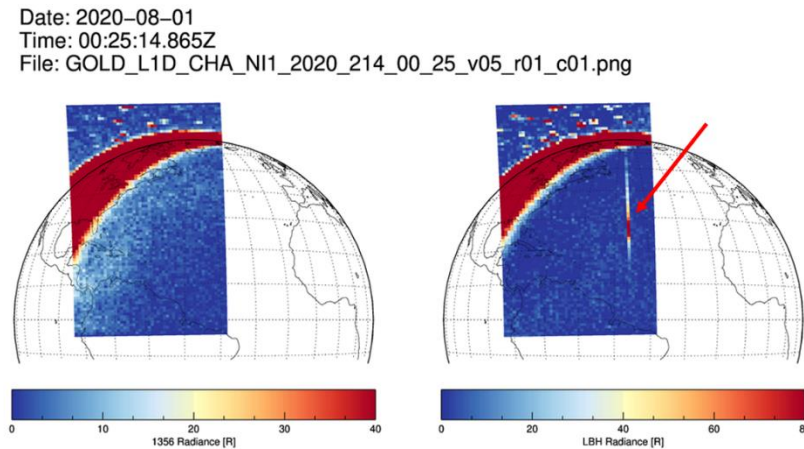
Figure 3-13 Example of field emission type events

3.1.17 Effect of stars on the brightness

When a star comes into the limb of the Earth, it appears as a bright spot in the image as shown in Figure 3-14. The starlight can scatter to pixels along the slit and can result in a bright vertical band in the image. These events are not flagged in the released data.
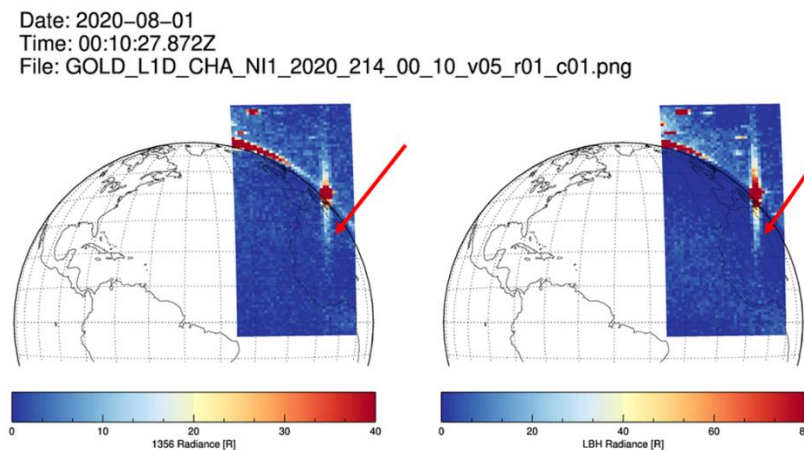
Figure 3-14 Scattering of starlight to pixels along the instrument slit

3.1.18 Horizontal artifacts in Channel B NI1 scans

In an effort to prolong the lifetime of the Channel B detector, Channel B primarily performs observations of the night disk in order to limit the detector's exposure to OI 135.6nm dayglow. This strategy works well for most of the detector, but it is impossible to avoid observing the bright auroral dayglow without giving up significant science. The result is that a few isolated rows of the

detector see significant degradation at the core of the OI 135.6nm emission. Typically, this degradation has little effect on science because it is isolated to rows of the detector which see the aurora and have limited scientific value. There are instances where the hemisphere that the Channel B instrument was observing was changed without an associated GYM move. The resulting artifacts appear as depleted (left panel, Figure 3-15) or enhanced (right panel, Figure 3-15) horizontal stripes in the OI 135.6 nm emission observations. These are not flagged in the released data. Table 3-2 summarizes times in the GOLD mission when this artifact may be present.
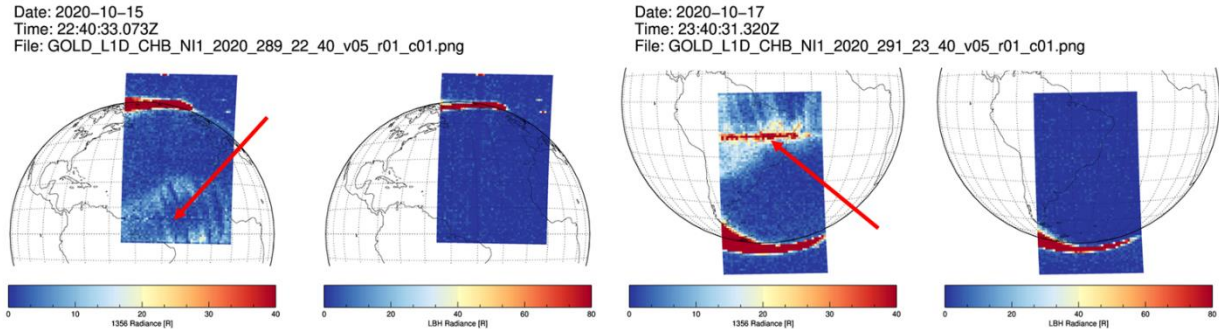
Figure 3-15 Horizontal stripes in Channel B NI1 scans due to limitations in the flat-field correction

Date Range	Description
10/04/2019-10/24/2019	Depletions observed in northern hemisphere scans
10/25/2019-11/30/2019	Enhancements observed in northern hemisphere scans
04/20/2020-05/12/2020	Weak enhancements observed in northern hemisphere scans
09/30/2020-10/19/2020	Enhancements observed in southern hemisphere scans; weak depletions observed in northern hemisphere scans
04/19/2021-04/23/2021	Strong enhancements observed in southern hemisphere scans
04/24/2021-05/30/2021	Weak enhancements continue in southern hemisphere scans
10/24/2022-11/08/2022	Enhancements observed in southern hemisphere scans
08/7/2023-08/31/2023	Weak enhancements observed in southern hemisphere scans

Table 3-2 Time periods with horizontal artifacts in CHB NI1 data

3.1.19 Artifacts in first DAY scan after an instrument safe-hold (or error recovery)

In rare cases, the GOLD instrument enters safe mode (e.g., when the bright object sensor is triggered). When the instrument is brought out of safe mode, the first DAY image scan may exhibit an artifact like in Figure 3-16, where a blue strip corresponding to zero radiance is seen on the right side of the image. This artifact occurs because the detector high voltage is not fully

ramped up when the scan starts. The high voltage ramps up rather quickly, and most of the scan is valid. However, the part of the image near the artifact should be disregarded. This artifact may also occur in the first DAY scan after observations are interrupted to perform an error detection and correction (EDAC) error recovery.
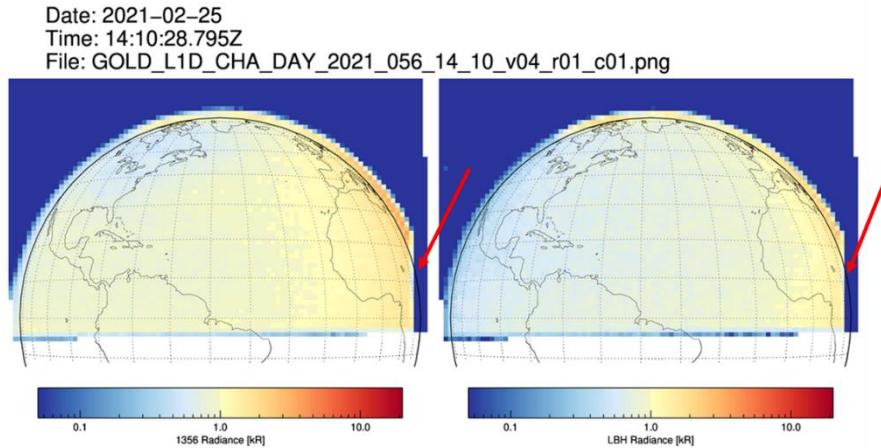
Figure 3-16 Artifact in DAY image after instrument safe-hold

3.1.20 Bad Airglow Subtraction for Select Stars

A select set of five observed stars are known to be problematic for the L1C processing algorithm which subtracts the airglow background. The algorithm uses the region of the detector above and below the observed star to remove background as detailed in section 4.4.2.4 of the GOLD Public Science Data Products Guide. When observing those five stars, listed in Table 3-3, there are nearby stars that are present in these regions of the detector causing the airglow subtraction algorithm to fail. Users should be cautious when using data products observing these stars.

Star Name	HD	RA	DEC	# Stars in FOV
eps Ori	HD37128	84.0532	-1.2019	5
iot Ori	HD37043	83.858	-5.9099	5
HR 1952	HD37756	85.211	-1.1289	5
HR 1861	HD36591	83.172	-1.5919	5
HR 1781	HD35299	80.9259	-0.1597	2

Table 3-3 List of stars that exhibit artifacts from bad airglow subtraction

3.2 Level 2

All GOLD Level 2 files contain arrays for three separate components of the total error in retrieved geophysical parameters – random, systematic, and model errors. The error characterization for some Level 2 data products in this release is still partially incomplete. Specifics for each data product are described in the sections that follow.

Each Level 2 data product file contains a list of data quality indices (DQI) specific to that product. These DQI are defined at both the file and individual pixel level and are described in detail in the **GOLD Science Data Product Guide** (available on the GOLD website)**.** That document also contains a description of each Level 2 data product, including a summary of the algorithm theoretical basis and a complete description of the contents of each Level 2 daily NetCDF file.

3.2.1 Issues with O2DEN data

3.2.1.1   Preliminary error analysis

A comprehensive error analysis and retrieval characterization for the O2DEN product is in progress but has not yet been implemented in this release. Currently only the random error array is populated in the O2DEN files. These errors should be considered preliminary until the detailed error analysis is implemented.

3.2.1.2   Valid altitude range in retrieved O_2 profile

The O2DEN data product – density profile of molecular oxygen (O_2) retrieved from stellar occultation (OCC) measurements – is retrieved on a fixed geometric altitude grid. However, the altitude range of the retrieved profile varies for each event (altitudes above and below the valid retrieval range for each event are populated by fill values). This is because the algorithm truncates the input measured atmospheric slant path transmission profiles to a fixed transmission range before input to the optimal estimation routine. A given transmission value will correspond to different tangent altitude levels as the absolute O_2 number density varies with geophysical conditions.

Pending a more complete retrieval characterization analysis to accompany the error analysis in a future release, a preliminary sensitivity study has been performed to characterize the degree of *a priori* bias in the O_2 retrievals. Figure 3-17 summarizes the results of this analysis. It shows the relative difference, in %, between the retrieved O_2 profile and the *a priori* profile for a random sample of ~500 occultations over 60 days. Difference profiles for the individual occultation events are shown in the left panel and daily averages are on the right. These plots clearly illustrate the behavior described above, with the retrieved O_2 converging to the *a priori* at both high and low altitudes. Based on this analysis it is recommended that users assign the highest confidence to the altitude region between 130 and 190 km, which contains the most independent

information on the absolute O_2 density profile. This range is denoted by the dashed horizontal lines in Figure 3-17. Currently the error bars and DQI reported in the O2DEN data files do not capture this data quality metric.
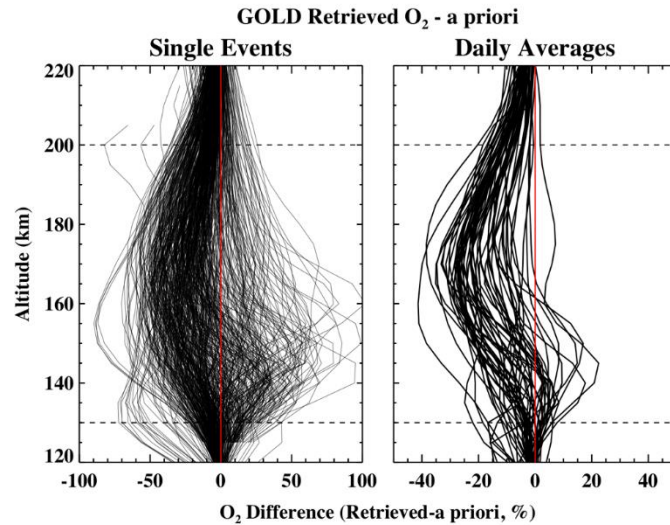

Figure 3-17 Variance between retrieved O2 profile and retrieval a priori.

3.2.1.3   Data gaps

There is a gap of approximately one month in the O2DEN data set, from December 17, 2018 to January 13, 2019. During this time period there was a glitch in the GOLD operational planning that caused errors in the instrument pointing and timing, resulting in missed occultations. This data is not recoverable since no underlying L1C data were obtained.

3.2.1.4   Potential bad airglow subtraction for select stars

As described in section 3.1.20 there is a set of 5 of the GOLD target stars that are known to be problematic for the L1C OCC data processing due to the presence of other nearby stars in the slit during the observations. Data from these stars should be used with caution. The TARGET_STAR parameter included in the L2 O2DEN files identifies the star name for each occultation and can be checked against the table in section 3.1.20.

3.2.1.5   Timing errors

As described in section 2.1.1, a correction has been applied to the GOLD L1 data to mitigate issues with instrument clock drift. As discussed in section 2.2.7 (O2DEN), this correction has greatly reduced issues with errors in the geometric altitude grid assigned to the retrieved O2 density profile in the O2DEN product.

Because this timing correction cannot be applied to GOLD data prior to January 30, 2019, O2DEN data prior to that date can still exhibit altitude errors associated with the timing errors.

3.2.2 Issues with TLIMB data

3.2.2.1   Preliminary error analysis

A comprehensive error analysis and retrieval characterization for the TLIMB product is in progress but has not yet been implemented in this data release. Currently only the random error array is populated with non-fill values in the Level 2 files. These errors should be considered preliminary until a more detailed error analysis is performed.

3.2.2.2   Stars in the field of view

It is common for stars to be observed within the field-of-view of the detector during limb scans. An example showing multiple stars within the field-of-view can be seen in Figure 3-18. When a star appears in the field-of-view it can alter the shape of the N_2 LBH limb profile producing systematic biases in retrieved exospheric temperatures. Therefore, the TLIMB algorithm code implements a star detection algorithm that utilizes the difference between stellar and airglow spectra. When a star is detected in the field-of-view the TLIMB algorithm is not run and the corresponding DQI is set to a non-zero value. Note that the star detection algorithm is not 100% reliable, thus false positive and negative detections may occur. Users are advised to independently review the Level 1C data for stars in the field-of-view when working with the TLIMB data.
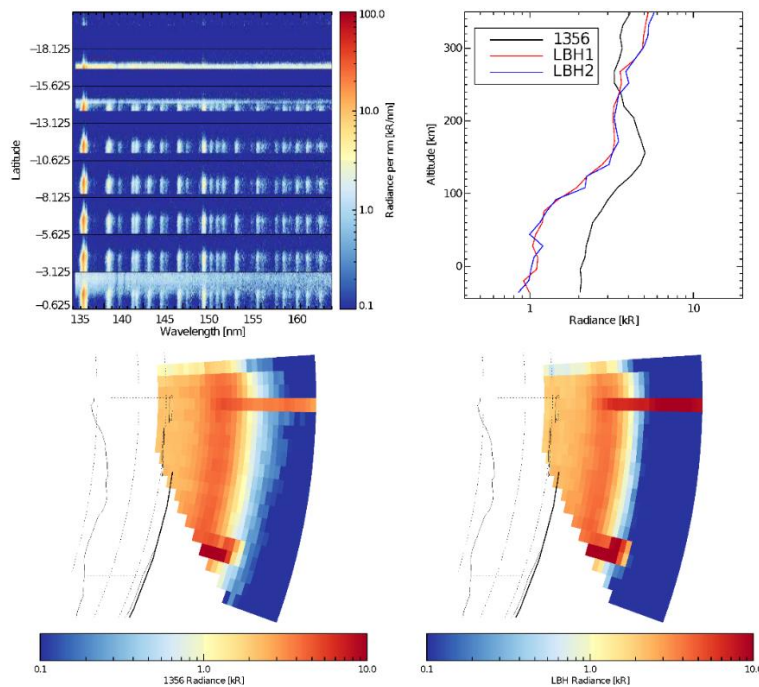

Figure 3-18 Level 1D plot showing observation of multiple stars in the field-of-view during a limb scan.

3.2.2.3   Latitude constraints

The signal-to-noise ratio at the edge of the detector (on the equatorward, north end of the slit) is typically low during southern hemisphere scans, which can produce systematic biases in retrieved temperatures. Therefore, the TLIMB algorithm is not run (TLIMB is set to fill value and DQI set to non-zero value) when the latitude of southern hemisphere limb scan data is greater than 2.5 degrees. Note that northern hemisphere scans may also be affected by low signal-to-noise at the edge of the detector (south end of the slit), though no latitude constraint is currently imposed for northern scans. Users are advised to use caution when working with TLIMB data derived from the edges of the detector.

3.2.2.4   Tangent altitude constraints

The TLIMB algorithm is only run if the tangent altitudes span the range from 250 km (or higher) to 160 km (or lower) and there are no NaNs in the corresponding Level 1C LIM brightnesses or uncertainties. If this condition is not met, the TLIMB value is set to a fill value and the corresponding DQI is set to a non-zero value.

3.2.2.5   Degraded performance at large solar zenith angle

When the solar zenith angle is between 60 and 90 degrees the TLIMB algorithm is run but a corresponding DQI is set to a non-zero value indicating the potential for degraded algorithm performance. The algorithm is not run when the solar zenith angle is greater than 90 degrees. Degradation at high solar zenith angles primarily affects the TLIMB data on the East limb as viewed from GOLD (positive longitudes in the Level 2 file). Users should apply extra caution when working with TLIMB data products when algorithm performance is degraded, particularly the data on the East limb at solar zenith angles greater than 70 degrees.

3.2.2.6   Algorithm failure

Occasionally the TLIMB algorithm will fail to converge when fitting an observed N_2 LBH limb profile. If the algorithm fails to retrieve an exospheric temperature the TLIMB value is set to a fill value and the corresponding DQI is set to a non-zero value.

3.2.2.7   Data gaps

There is a gap of one day in the TLIMB data for October 9, 2018, when the TLIMB retrievals are anomalously high. This could be related to high particle background levels on that day, although this is inconclusive at this time.

3.2.3 Issues with TDISK data

3.2.3.1   Preliminary error analysis

A comprehensive error analysis and retrieval characterization for the TDISK product is in progress but has not yet been implemented in this data release. Currently only the random error array is populated with non-fill values in the Level 2 files. These errors should be considered preliminary until a more detailed error analysis is performed.

3.2.3.2   Algorithm limits

The TDISK algorithm code is not run when the solar zenith angle exceeds 80 degrees, or the emission angle exceeds 75 degrees.

3.2.3.3   Algorithm failure

Occasionally the TDISK algorithm will fail to converge when fitting an observed spectrum. If the algorithm fails to retrieve an effective neutral temperature the TDISK value is set to a fill value and the corresponding DQI is set to a non-zero value.

3.2.3.4   Effective altitude.

As with any satellite nadir (disk) viewing measurement, the GOLD DAY disk observations sample all altitudes along a given line of sight, from the top of the atmosphere to below the peak of the emitting layer. The observed temperatures are weighted by the peak volume emission rate at altitudes where there is a significant temperature gradient (~150-200 km). Since the GOLD disk observations represent a column integration of the weighting function (i.e., there is no altitude information), the effective height of the derived TDISK temperature product, which varies with viewing conditions (solar zenith angle and, to a lesser extent, emission angle) must be determined with the aid of forward modeling. This work has not yet been completed as of present release and thus we report a default value of NaN for the effective altitude. We note for clarity that previous data versions recorded a value of 150 km for the TDISK effective altitude. This reference altitude level is used to geolocate pixels for the GOLD DAY disk data, however the reported TDISK values are not intended to be representative of this altitude.

3.2.3.5   Sources of contamination

One potential source of contamination that may produce artifacts in the TDISK retrieved temperatures is energetic particle flux in the polar regions. At present, there is no auroral boundary detection algorithm implemented in the Level 2 operational pipeline, and users are therefore advised to use caution when working with TDISK data when the geomagnetic latitude exceeds 60 degrees.

3.2.3.6   Discontinuities around GYM actuations

As discussed in Section 3.1.1, an operation called a GYM actuation is occasionally implemented to mitigate the effects due to detector burn-in (the GYM actuation dates are listed in Table 3-1). The TDISK data can exhibit discontinuities before and after the GYM actuation operations, as illustrated in Figure 3-19. This artifact primarily affects TDISK around the first, fourth, and fifth GYM actuations (4/26/2019, 8/11/2020, and 2/8/2021). TDISK values show an immediate drop or increase after these dates, with a recovery time ranging from ~5 to 15 days. Caution is advised when using the TDISK data for times near any GYM actuation operation.
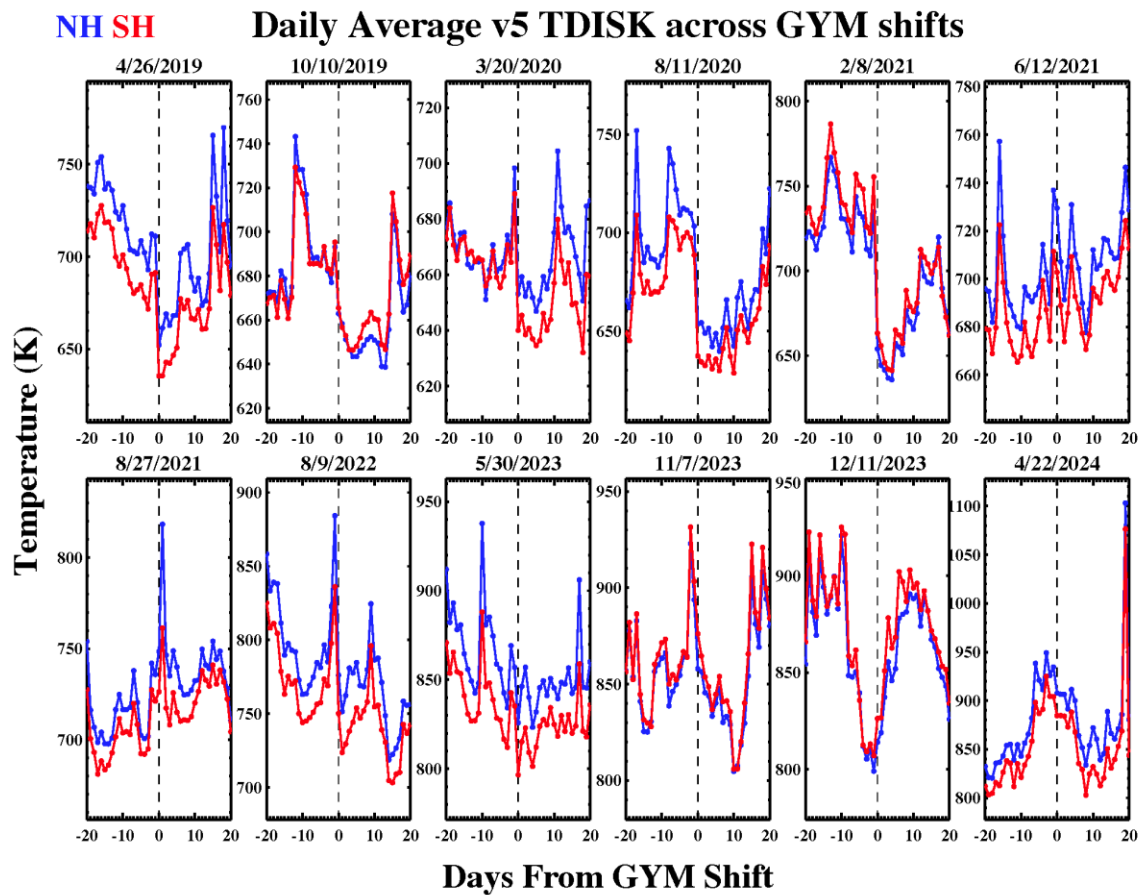

Figure 3-19 Daily average TDISK v05 data before and after the Channel A GYM shift operations to date. Northern/Southern hemisphere (NH/SH) are plotted in blue and red, respectively. In each panel the vertical line is the date of the GYM operation.

3.2.4 Issues with ON2 data

The primary issues affecting ON2 data quality are related to the degradation of measured O I 135.6 nm emission brightness due to detector burn in. The impact of these artifacts in the ON2 data can vary with season and time of day, depending on the state of the instrument and the

effectiveness of corrections used to mitigate detector burn-in. End users are advised to exercise caution when interpreting ON2 values during times of increased L1C data artifacts described below. ON2 is most useful as a measure of relative changes in the atmosphere, and it is suggested that users apply analysis techniques that tend to minimize effects due to instrument artifacts, e.g., taking deviations relative to a daily mean, or differencing the same times during consecutive days. Direct comparison of ON2 values over large time differences (more than several days) require particular care.

3.2.4.1   Algorithm limits

The $\Sigma O/N_2$ algorithm is not run when the solar zenith angle is greater than 80 degrees or the emission angle is greater than 75 degrees.

3.2.4.2   Contamination of ON2

The $\Sigma O/N_2$ algorithm assumes the only source of O I 135.6 nm and N_2 LBH emissions are photoelectrons generated by solar EUV flux. Other sources of these emissions are considered contaminants and will result in erroneous derived $\Sigma O/N_2$ values. The main sources of the contaminant emissions for the $\Sigma O/N_2$ algorithm are energetic particle precipitation in the polar regions (affecting both 135.6 nm and LBH) and radiative recombination of O^+ in the equatorial ionization anomalies (affecting only 135.6 nm). At present, there is no auroral boundary detection algorithm implemented in the Level 2 operational pipeline, therefore users are advised to use caution when working with ON2 data where the geomagnetic latitude exceeds 60 degrees. Similarly, users are advised to use caution when working with ON2 data during geomagnetically active periods that may produce enhanced radiative recombination emission in the equatorial ionization anomalies.

3.2.4.3   Hemispheric bias

The residual gradient in instrument sensitivity described in Section 3.1.2 causes small biases in the measured radiances in the along-slit direction (essentially North-South). This artifact is greatest at short wavelengths, and hence affects the oxygen 135.6 nm band brightness more than LBH. These radiance biases produce similar biases in the derived ON2 values (even though ON2 is derived from the ratio of 135.6 nm and LBH band intensities, the wavelength dependence of residual, along-slit sensitivity biases means that the effect does not cancel). The largest manifestation of this effect is seen in ON2 derived near the equator, since these pixels are sampled by opposite ends of the slit in the Northern hemisphere (NH) and Southern hemisphere (SH) scans. The net result is an offset of approximately 1-3% on average in ON2 (NH higher than SH) at the equator. This will show up as a banding artifact along the equator in a full global ON2 image created from consecutive NH and SH scans. Note that this artifact has been significantly reduced in the v04 ON2 product, and generally only appears near the GYM actuations early in the GOLD mission.

3.2.4.4 Discontinuities around GYM actuations

As discussed in Section 3.1.1, an operation called a GYM actuation is occasionally implemented to mitigate the effects due to detector burn-in (the GYM actuation dates are listed in Table 3-1). The ON2 data sometimes exhibits discontinuities immediately before and after this operation, driven primarily by abrupt changes in the 135.6 nm radiance, as illustrated in Figure 3-20. This artifact is evident in the ON2 data to some extent at all GYM actuations. ON2 values immediately before and after these operations show a difference in overall magnitude as well as distinctly different local time dependence throughout the day (not shown in Figure 3-20). Caution is advised when using the ON2 data for times near any GYM actuation operation, particularly earlier in the mission (i.e., the first 5 GYM actuations).
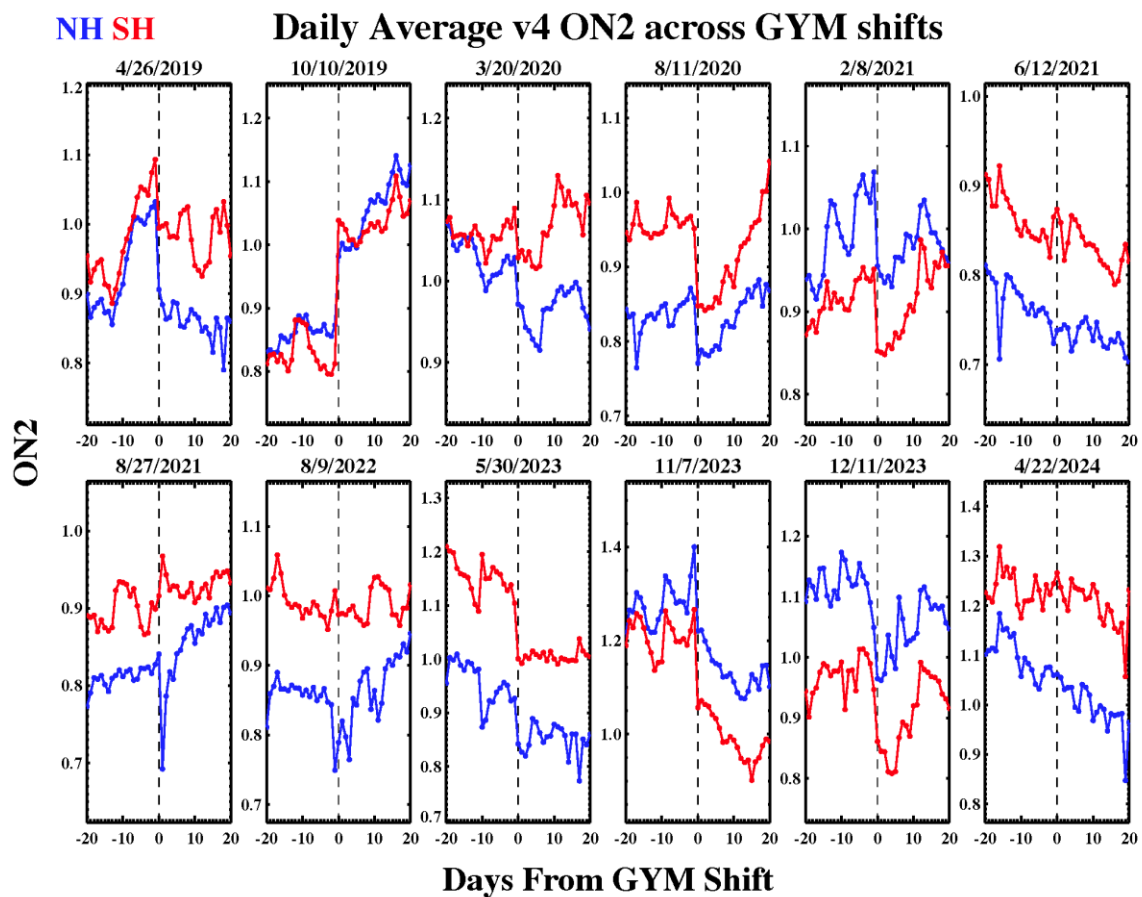

Figure 3-20 Daily average v04 ON2 data before and after the Channel A GYM shift operations to date. Northern/Southern hemisphere (NH/SH) are plotted in blue and red, respectively. In each panel the vertical line is the date of the GYM operation.

3.2.4.5 Flat Field correction artifacts

The flatfield correction has some limitations that affect ON2. As discussed in Section 3.1.5 the flatfield correction can sometimes under- or over-correct data depending on time of day and

season. Errors in the flatfield correction are largest in the 135.6 nm band during periods when a significant correction is needed, such as the weeks preceding a GYM actuation. These errors can appear as biases and/or enhanced scatter in the ON2 data. See Figure 3-21, where the flatfield correction errors result in horizontal bands of depleted (left) or enhanced (right) $\Sigma O/N_2$ just below the equator.
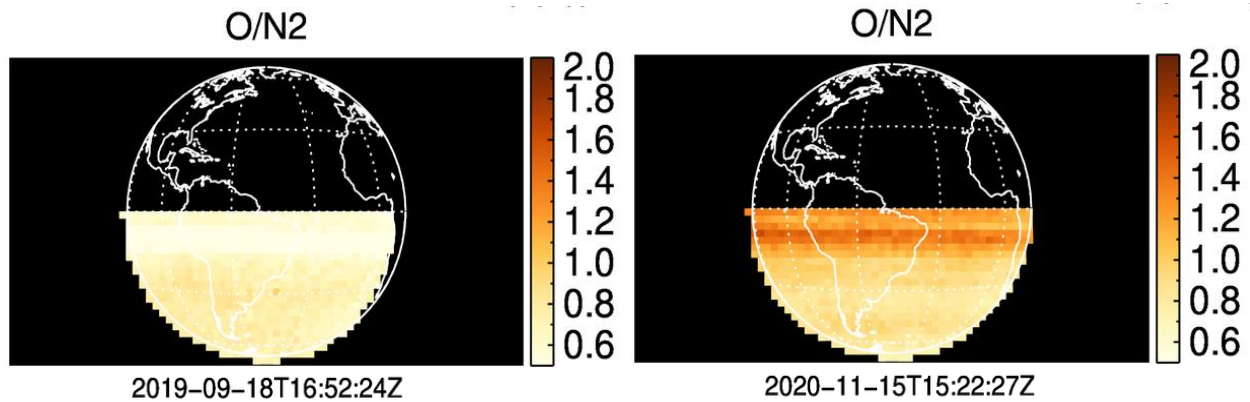

Figure 3-21 Examples of the impact of flat field correction errors on the ON2 data product. The errors result in horizontal bands of depleted (left) or enhanced (right) O/N$_2$

3.2.4.6 ON2 Artifacts during May 20-25, 2023 (DOY 140-145)

The Level 2 ON2 data exhibits some artifacts during the period of May 20-25, 2023 (DOY 140-145). This is assumed to be related to issues in the underlying L1C data, but the exact cause is currently under investigation. In the meantime, caution is advised when using the ON2 data in this time period.

3.2.5 Issues with QEUV data

Like ON2, the QEUV parameter is derived from measurements of the O I 135.6 nm and N$_2$ LBH emission radiances. The primary issues affecting QEUV data quality are sensitivity to instrument degradation, flat field corrections, and other effects, particularly with the 135.6 nm intensities.

3.2.5.1 Algorithm limits

QEUV values are not derived where the solar zenith angle is greater than 80 degrees or the emission angle is greater than 75 degrees. Furthermore, QEUV is only derived for DAY disk scan is between 10- and 20-hours UTC.

3.2.5.2 Contamination of QEUV

As with ON2, the QEUV algorithm assumes the only source of O I 135.6 nm and N$_2$ LBH emission is photoelectrons generated by solar EUV flux. Other sources of these emissions are considered contaminants and will result in erroneous derived QEUV values. The main source of the contaminant emissions for the QEUV algorithm is radiative recombination of O$^+$ in the

equatorial ionization anomalies (affecting only 135.6 nm). Users are advised to use caution when working with QEUV data during geomagnetically active periods that may produce enhanced radiative recombination emission near the equatorial ionization anomalies.

3.2.5.3   Hemispheric bias

There is a small bias between the QEUV values derived from near-coincident Northern Hemisphere (NH) and Southern Hemisphere (SH) scans. This bias has a seasonal component, with SH values higher than NH from ~March through September and changing signs the rest of the year. The magnitude of the difference ranges from a maximum of ~10% (SH > NH) in NH summer to ~5% (SH < NH) in NH winter. Part of this issue is related to the gradient in instrument sensitivity along the slit described in Section 3.1.2. As with the ON2 data product, the North/South bias in the measured 135.6 nm radiances propagates into the QEUV retrieval. The seasonal component of this bias in QEUV seems to another possible source of error that is under investigation.

3.2.5.4   Discontinuities around GYM actuations

As discussed in Section 3.1.1, an operation called a GYM actuation is occasionally implemented to mitigate the effects due to detector burn-in (the GYM actuation dates are listed in Table 3-1). The QEUV data exhibits discontinuities immediately before and after the GYM actuation operations, driven primarily by abrupt changes in the 135.6 nm radiance. This is illustrated in Figure 3-22. The artifact is most significant in QEUV at the first, fourth and fifth GYM actuations, and to a much lesser or negligible extent at the others. QEUV values immediately before and after these operations show a jump in magnitude. Caution is advised when using the QEUV data for times near any GYM actuation operation.
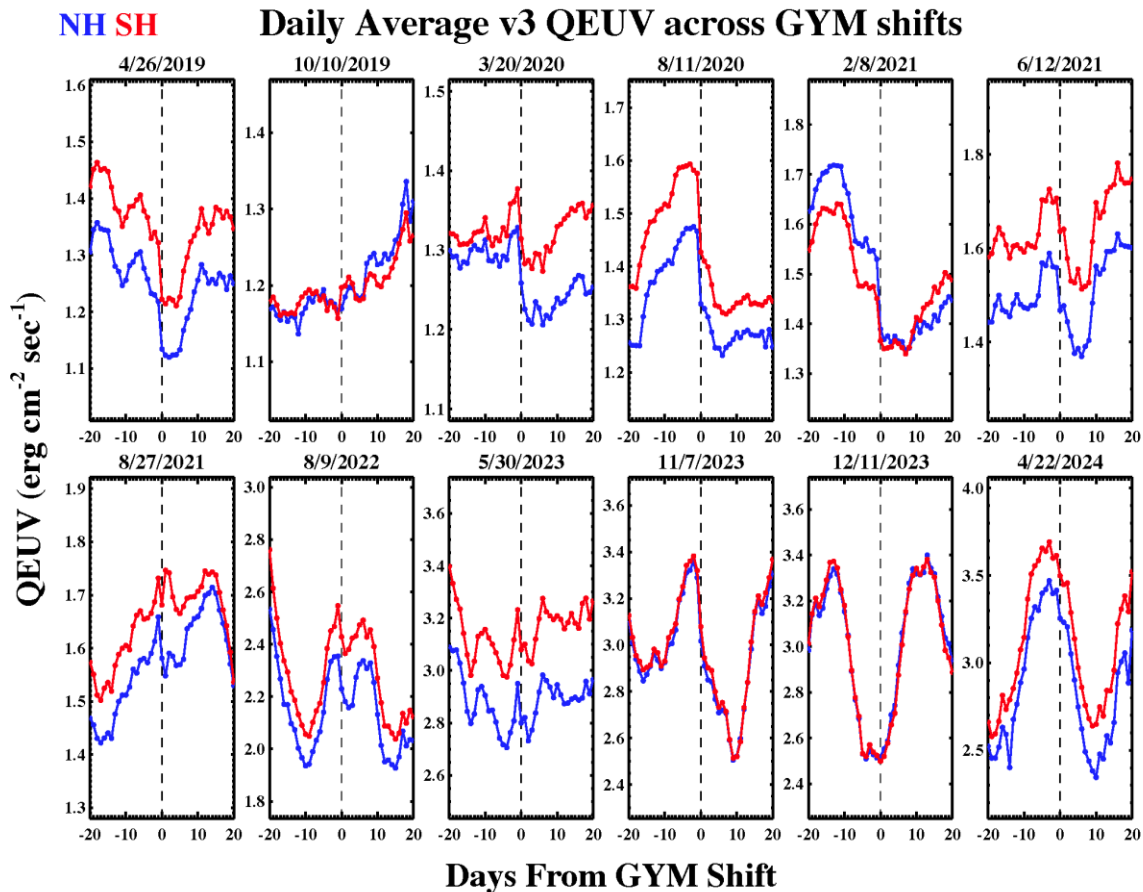
Figure 3-22 Daily average v03 QEUV data before and after the Channel A GYM shift operations to date. Northern/Southern hemisphere (NH/SH) are plotted in blue and red, respectively. In each panel the vertical line is the date of the GYM operation.

3.2.5.5   Flat Field correction artifacts

The flatfield correction has some limitations that affect QEUV. As discussed in Section 3.1.5 the flatfield correction can sometimes under- or over-correct data depending on time of day and season. Errors in the flatfield correction are largest in the 135.6 nm band during periods when a significant correction is needed, such as the weeks preceding a GYM actuation. These errors can result in biases and/or enhanced scatter in the QEUV data during these periods.

3.2.6 Issues with NMAX data

3.2.6.1   Model uncertainty

Because the current NMAX algorithm neglects two sources of 135.6 nm photons (ion-ion mutual neutralization: $O^+ + O^- \rightarrow O + O + h\nu$ and resonant scattering of 135.6 nm photons by atomic oxygen), it tends to overestimate the value of NMAX. We estimate that the model error due to

the omission of these two sources is approximately 15% (that is +15% and −0%) depending on several variables mainly having to do with atmospheric composition and variability in the electron density profile shape.

3.2.6.2 Flat Field correction artifacts

On some days, the flat-field correction may introduce horizontal artifacts in the L1C CHB NI1 images (see section 3.1.18). These artifacts will also propagate through to the L2 CHB NMAX data, as seen in the example in Figure 3-23 below. These are not flagged in the data.
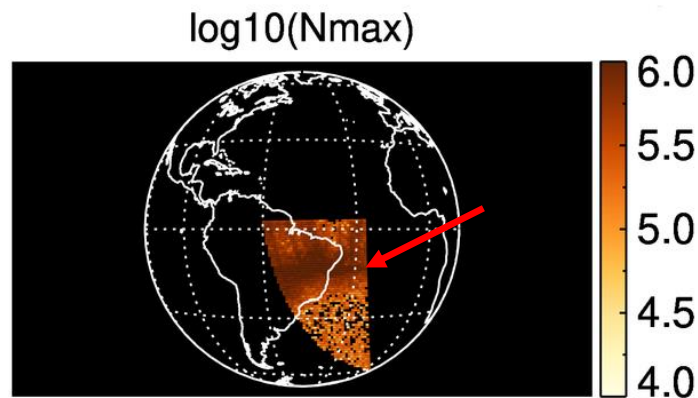

Figure 3-23 Horizontal stripe in the CHB NMAX data due to issues in the flat-field correction of the L1C NI1 data.

3.2.6.3 Data Gaps

There is a large data gap in the Channel B data between Dec 15, 2018 and Mar 15, 2019 due to a detector burn in problem, which renders the Channel B NI1 data taken during that time useless for quantitative analysis, such as retrieving NMAX. The Channel A data for this period is useable.

4 Upcoming Work / Plan for Upcoming Releases

4.1 Level 1

Add wavelength dependent shape to scattered light background subtraction

Release of additional CHB data products

Quality flags for stars and moon in field of view

Quality flag for presence of xenon emission feature

4.2 Level 2

Better characterization of some error components on retrieved geophysical parameters.

Apply additional spatial binning to the QEUV algorithm to reduce data scatter.

Implement an auroral boundary detection algorithm.

5 References

Ajello, J. M., Evans, J. S., Veibell, V., Malone, C. P., Holsclaw, G. M., Hoskins, A. C., et al. (2020). The UV spectrum of the Lyman-Birge-Hopfield band system of N2 induced by cascading from electron impact. Journal of Geophysical Research: Space Physics,125, e2019JA027546, https://doi.org/10.1029/2019JA027546.

McClintock, W. E., Richard W. Eastes, Alan C. Hoskins, Oswald H.W. Siegmund, Jason B. McPhate, Andrey Krywonos, Stanley C. Solomon, and Alan G. Burns (2020), Global-scale Measurements of the Limb and Disk (GOLD) Mission Implementation: 1. Instrument Design and Early Flight Performance, *J. Geophys. Res. Space Physics*, *125*, e2020JA027797, https://doi.org/10.1029/2020JA027797.

McClintock, W. E., et al. (2020), Global-scale Measurements of the Limb and Disk (GOLD) Mission Implementation: 2. Observations, Data Pipeline and Level 1 Data Products, *J. Geophys. Res. Space Physics*, *125*, e2020JA027809, https://doi.org/10.1029/2020JA027809.

Aryal, S., S. Evans, J. M. Ajello, S. C. Solomon, A. W. Burns, R. W. Eastes, W. E. McClintock (2022), Constraining the upper level vibrational populations of the N2 Lyman-Birge-Hopfield Band System using GOLD mission's day glow observations, Journal of Geophysical Research: Space Physics, 127, e2021JA029869, https://doi.org/10.1029/2021JA029869.